# ERS-2 Wind Scatterometer Cyclic Report

from24th January 2000 to 28th February 2000
Cycle 50

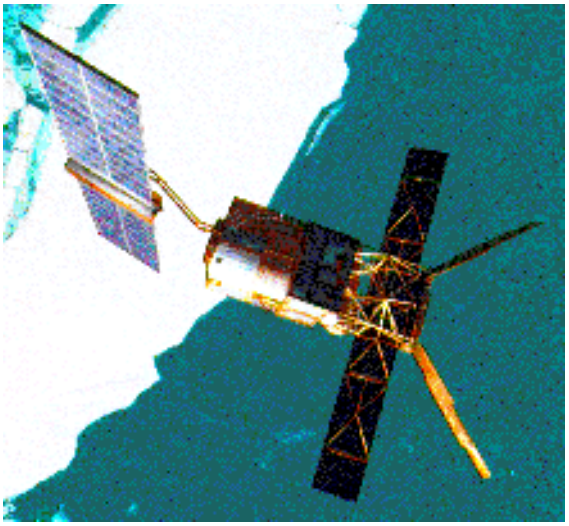


| | | |
|---|---|---|
| Prepared by: | PCS team | ESRIN APP-ADQ |
| Inputs from: | F. Aidt | ESTEC TOS-EMS |
| | L. Isaksen | ECMWF |



Document No: APP-ADQ/PCS/WS00-003
Issue: 1.0
Date: 20th, March 2000

# Distribution List

| | | |
|---|---|---|
| ESAHQ | G. Duchossois | |
| ESTEC | M. Canela | APP-LR |
| | E. Attema | SCI-VRS |
| | F. Aidt | TOS-EMS |
| | B. Gelsthorpe | APP-LTP |
| | R. Zobl | |
| | K. van't Klooster | |
| ESOC | F. Bosquillon de Frescheville | TOS-OFC |
| | L. Stefanov | TOS-OFC |
| ESRIN | M. Albani | APP-AD |
| | P. Lecomte | APP-ADQ |
| | V. Beruti | APP-ADF |
| | S. Jutz | APP-ADU |
| | G. Kohlhammer | APP-AM |
| | M. Onnestam | APP-ADC |
| | U.Gebelein | Serco |

| | |
|---|---|
| L.A. Breivik | DNMI |
| P. Snoeij | DUT |
| J. Heidbreder | DORNIER |
| L. Isaksen | ECMWF |
| J. Kerkman, J. Figa | EUMETSAT |
| S. Pouliquen | F-PAF |
| V. Wismann | IFARS |
| A. Cavanie | IFREMER |
| R.S. Dunbar | JPL |
| A. Stoffelen, T. Driessenaar | KNMI |
| G. Legg, P. Chang | NOAA/NESDIS |
| W. Gemmill | NOAA/NWS |
| J. Hawkins | NRL |
| D. Offiler, R. Graham, C.A. Parrette | UK-MET Office |
| F. Courtier, H. Roquet | Meteo-France |
| C. Scupniewicz | FNMOC |
| R.A. Brown | University of Washington |
| J. Boutin | LODYC/UPMC |

This report and its annex are also available via FTP.
ftp pooh.esrin.esa.it (login as anonymous)
cd pub/SCATTEROMETER
wscatt_rep_50.ps.Z, annex_rep_50.ps.Z

# 1.0 Introduction and summary

The results reported in each section concern, apart from a summary of the daily quality control made within the PCS, the investigations and the study of “open-problems” related to the scatterometer, e.g. the CMOD-4 for high wind speed, the antenna pattern. In each section results are shown from the beginning of the mission in order to allow comparisons and to outline possible “seasonal” effects. An explanation of the major events that have impacted the performance since launch is given, and a comment about the recent events during the last cycle is included.

The most important event during the cycle 50 (from 24$^{th}$ January 2000 to 28$^{th}$ February 2000) has been the up-link on board ERS-2 of a new software to control the attitude of the satellite. The old Attitude On-board Control System (AOCS) configuration (one Digital Earth Sensor - DES, one Digital Sun Sensor - DSS and 3 gyros) is no more considered safe because 3 of the six gyros on-board are out of order or very noisy.

The new attitude control configuration is designed to pilot the ERS-2 using only one gyro plus the DES and the DSS modules. Scope of this new AOCS configuration is to extend the satellite life-time by using the available gyros one at the time. After the software up-link (7$^{th}$ February 1999) a two weeks of qualification period has been carried out using the gyroscope number 6 (first) and then the gyroscope number 5. After the qualification period the new AOCS (with gyro number 5) is piloting the ERS-2 satellite.

In theory the impact of the mispointing is know as being an error in the sigma nought estimation. A change in the antennae pointing causes a change in the doppler frequency and a shift of the signal spectrum (Centre of Gravity). In this situation the receiver bandwidth is not matched for the input signal spectrum and the result is an error in the sigma nought estimation. For this reason in the qualification period analysis has been carried out on the evolution of the CoG of the received spectrum and on the sigma nought This report summarises the preliminary results.

To monitor the pointing error the mean CoG has been computed during one orbit. The reason of this choice is because the CoG is related via the geometry with the evolution of the pointing error. The result with the old AOCS configuration is a very clean sinusoidal signal (that means, apart from the variation due to the orbit, very low value for the pointing error angles) while for the new configuration the result is in agreement with the sinusoidal pattern but with more noise in the shape. Moreover the gyro 5 goes away from sinusoidal pattern around 1500 seconds after the ascending node (North pole). This behaviour of the CoG is very well correlated with the error angles provided by ESOC.

The new AOCS configuration is more sensible to the Sun blinding. In fact the CoG shows a high fluctuation near the end of the orbit (around 5000-5500 s. from the ascending node) with an increase of the error pointing. This increase is due to the Sun blinding. In the South hemisphere, during the ascending passes, the Earth Sensor is blinding by the Sun light and switched off for few seconds causes the high pointing error. In the old AOCS configuration sun blinding data were discarded because the AOCS had 3-gyro as independently information but in the mono-gyro configuration they are used. The Sun blinding is a seasonal effect and it is not a strong reason to reject the new AOCS configuration. Its maximum is expected every year during the period 12$^{nd}$ January 26$^{th}$ February and with the new AOCS configuration it has a local impact in the sigma nought acquired in the South hemisphere. The Ocean calibration shows that there is up to 1 dB of variation in that area (far range nodes only ascending passes).

On average the new AOCS (gyro 6) had caused a decrease (w.r.t. the 3-gyro) of the daily mean of the CoG of roughly 200 Hz (300Hz for the aft antenna) while the AOCS with the gyro 5 had caused an increase (w.r.t 3-gyro) of roughly 150 Hz (3 antennae).

To monitor the calibration performance the following actions have been carried out:

- comparison between the antenna pattern computed over the rain forest during the qualification period with the antenna patterns computed for the same relative tracks during the years 1997, 1998, 1999.
- computation of the sigma nought evolution over the rain forest per node and per relative track since 1997.
- comparison of the gamma nought histograms over the rain forest during the qualification period with the histograms computed for the same relative tracks during the years 1997, 1998, 1999.
- increase of the calibration passes over the transponder during the qualification period.

The preliminary result for the calibration over the natural test site (rain forest) is stable. The new AOCS did not cause a change in the relative level of the signal and the antenna patterns computed during the qualification period are very close to the ones computed in the previous years The position of the maximum of the gamma nought histograms during the qualification period (2 weeks), is very close to the one computed for the same relative tracks during the years 1999, 1998 and 1997 and the small difference are within the variability of the rain forest. The shape of the histograms computed during the qualification period (2 weeks) is slightly more noisy in particular for the ascending passes. This confirm the behaviour noted in the weekly histograms but we need more observation to conclude that the small change in the histogram' s shape is due to the new AOCS configuration or it is a geophysical effect.

For the absolute calibration (transponders) the results are not available.

For the wind quality the analysis carried out in the PCS show that the speed bias and its standard deviation (UWI vs ECMWF forecast) are not changed. The ambiguity removal rate was above 92% before and during the qualification period. Low quality in the wind data has been detected on days 16$^{th}$ and 17$^{th}$ February when the Satellite was piloting in Fine Pointing Mode (FPM) that is less accurate than the nominal mode.

The ECMWF has given a strong support in the monitoring of the wind performances during the qualification period. The results are very stable and no changes are detected in the wind biases (speed and direction) as well as in the sigma nought distance from the cone. A deep analysis in the area 45-55 degrees South is on-going to evaluate the impact of the satellite mispointing on the wind quality.

As usual the report is available via ftp (login as anonymous) to the address pooh.esrin.esa.it directory /pub/SCATTEROMETER file names wscatt_rep_50.ps.Z, annex_rep_50.ps.Z (Unix compressed) and on the PCS web site: http://pcswww.esrin.esa.it (Scatterometer performance page). The statistics about the availability of the ERS-2 Wind Scatterometer raw data during cycle 50 and the detailed list of the unavailability periods are given in the document "ERS-2 AMI/RA/ATSR/GOME availability statistics" issued at the end of each cycle. Post processed Scatterometer data acquired over tropical cyclones are available on the web site: http://www.pcswww.esrin.esa.it (cyclone tracking page).

# 2.0 Calibration Performances

The calibration performances are estimated using three types of target: a man made target (the transponder) and two natural targets (the rain forest and the ocean). This approach allow us to design the correct calibration using a punctual but accurate information from transponders and an extended but noisy information from rain forest and ocean for which the main component of the variance comes from the geophysical evolution of the natural target and from the backscattering models used. These aspects are in the calibration performance monitoring philosophy. The major goals of the calibration monitoring activities are the achievement of a “flat” antenna pattern profile and the assurance of a stable absolute calibration level.

## 2.1 Gain Constant over transponder

One gain constant is computed per transponder per beam from the actual and simulated two-dimensional echo power, which is given as a function of the orbit time and range time. This parameter clearly indicates the difference between “real instrument” and the mathematic model. In order to acquire data over the transponder the Scatterometer must be set into an appropriate operational mode that is defined as “Calibration”.

Table 1 shows the result of the calibration plan for cycle 50. The “Yes” in the EWIC column means that the raw data are available, “No” means the opposite case. The “On” in the transponder status column means that, from the raw data (EWIC), the transponders has been recognised as switched-on; “Off” means the opposite case. The “Yes” in the GC computed column means that a gain constant value has been retrieved, “No” means the opposite case.

During the cycle 50 to monitoring the pointing of the ERS-2 satellite new calibration passes have been added. Table 1 summarises the status of the calibration plan. As reported in the table no new gain constants have been computed by ESTEC.

**TABLE 1. Calibration Plan: Cycle 50**

| DATE | ORBIT (absolute) | ORBIT (relative) | Passage | Ground Station | EWIC (raw data) | AMI mode | Transponder Status | GC computed |
|---|---|---|---|---|---|---|---|---|
| 000212 | 25177 | 273 | A | MS | Yes | Calibration | On | No |
| 000213 | 25184 | 280 | D | KS | Yes | Calibration | On | No |
| 000215 | 25220 | 316 | A | MS | Yes | Calibration | OFF | n/a |
| 000218 | 25263 | 359 | A | MS | Yes | Calibration | OFF | n/a |
| 000222 | 25320 | 416 | A | MS | No | Calibration | n/a | n/a |
| 000223 | 25327 | 423 | D | KS | No | Calibration | n/a | n/a |

Figure 1 and Figure 2 show the gain constants available since the beginning of the mission, the analysis is split for the different antenna elevation angle. From these figure it is clear that the gain constant measurements are stable (within +/-0.5 dB) but after the end of the commissioning phase (cycle 11) only few data are available.

The plots in Figure 3 show the value of the Gain Constant for the three beams and for the ascending, descending and all passes. The plots show the average of all gain constant available since January 1996 (cycle 8) for each antenna elevation angle. The antenna patterns are flat but there is a clear shift of the level of the curves. On average, the mid beam is 0.3 dB higher than the aft one and 0.5 dB higher than the fore one. For the descending passes the antenna pattern shows a slight negative slope from far range to near range.

Since September 1996 ESTEC has added a scaling factor to the gain constant in order to remove the bias among the three antennae. The gain constants were increased by 0.2 dB, -0.3 dB and 0.2 dB, for the fore, mid and aft beam respectively. The result is shown in figure 4. The suggestion given by ESTEC has not been introduced into the ground processing because the antenna patterns computed over the rain forest do not show such bias (see Figure 7). So in the actual scenario, the differences among the antennae are considered as a bias due to the transponder themselves.

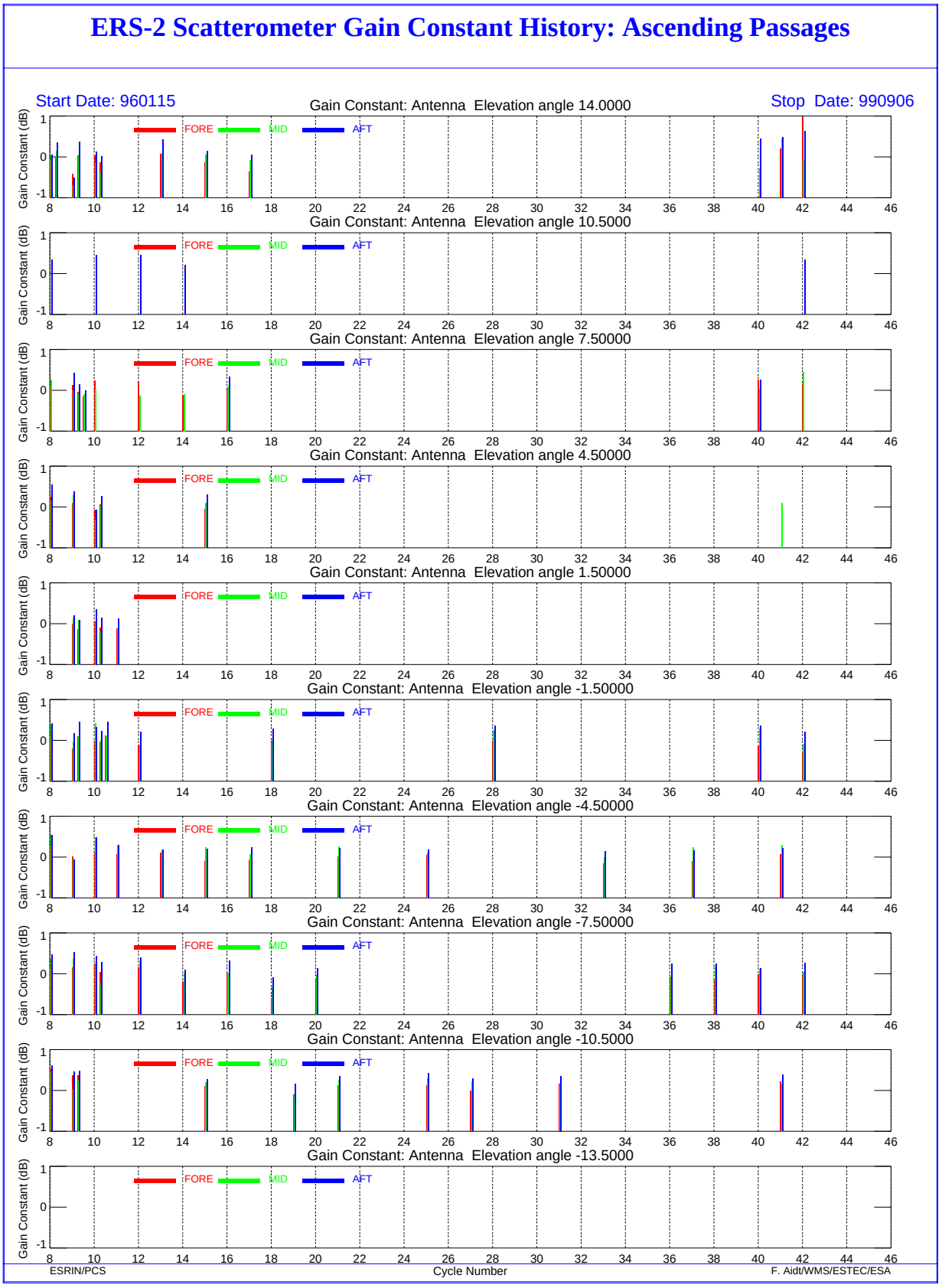


**FIGURE 1. ERS-2 Scatterometer; gain Constant over transponder since the beginning of the mission (ascending passes).**

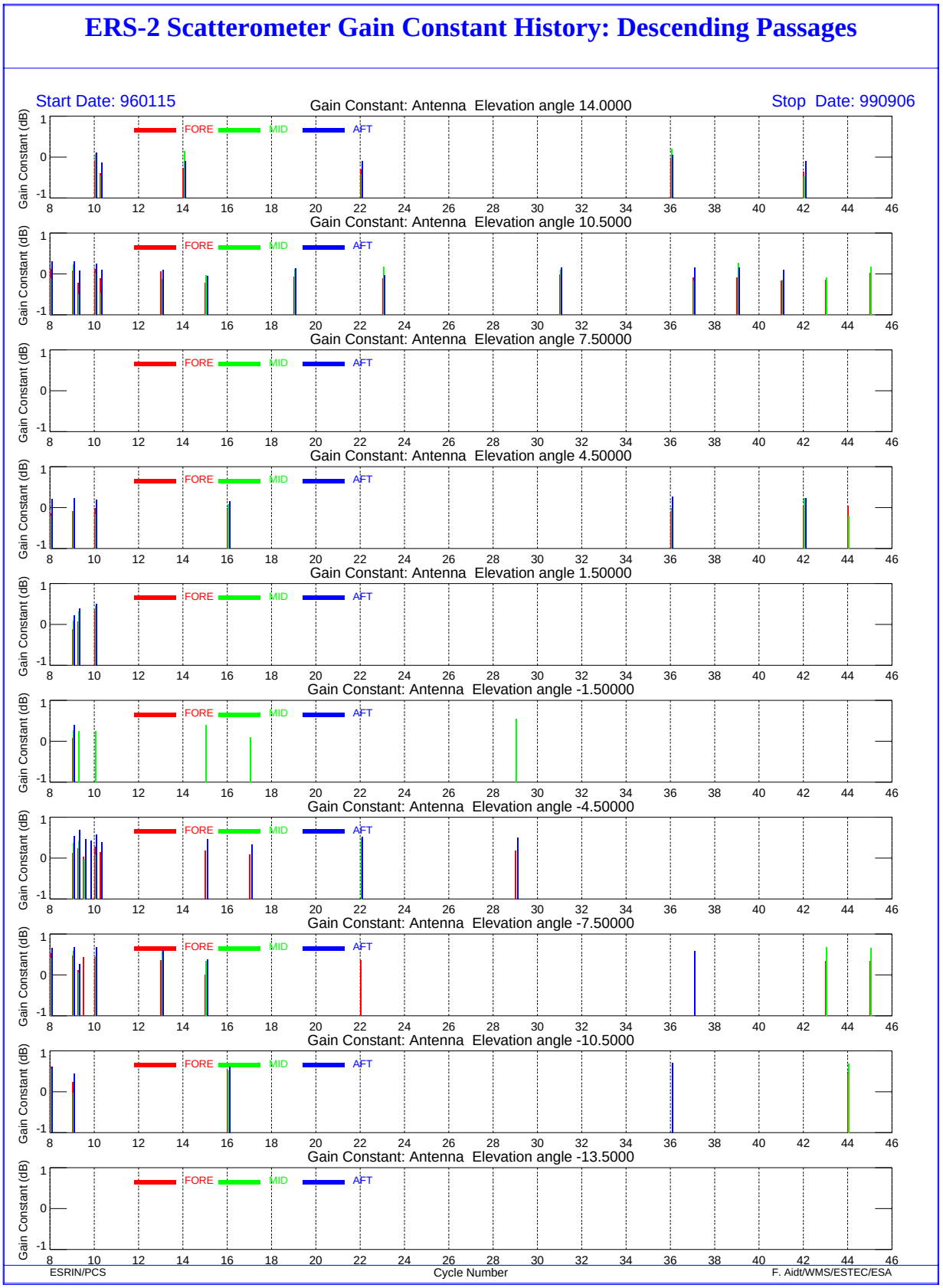


**FIGURE 2. Scatterometer; gain Constant over transponder since the beginning of the mission (descending passes)**

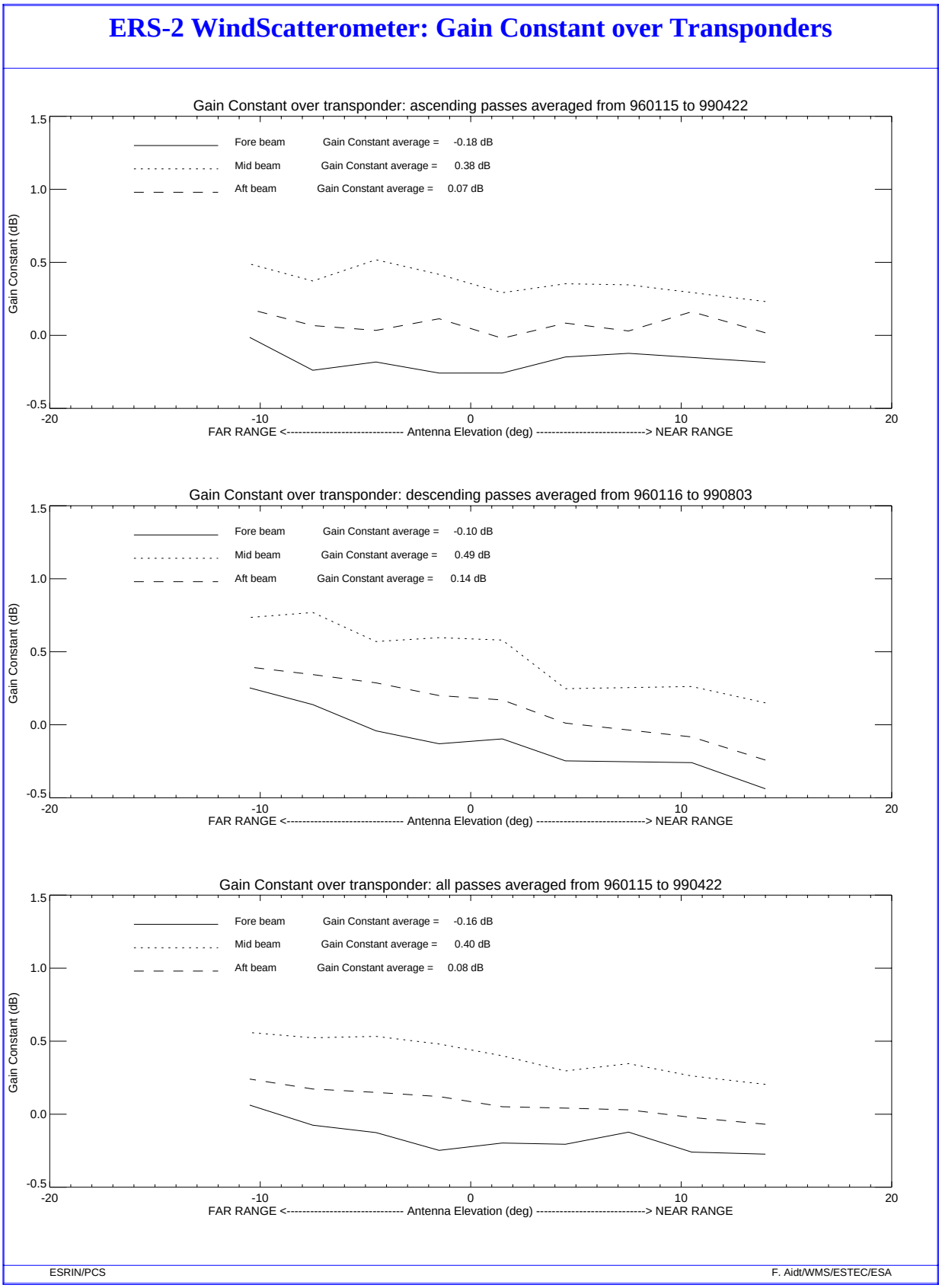


**FIGURE 3. ERS-2 Scatterometer: gain constant over transponders. All data available since January 1996. Upper plot: ascending passes. Middle plot: descending passes. Lower plot: all passes.**

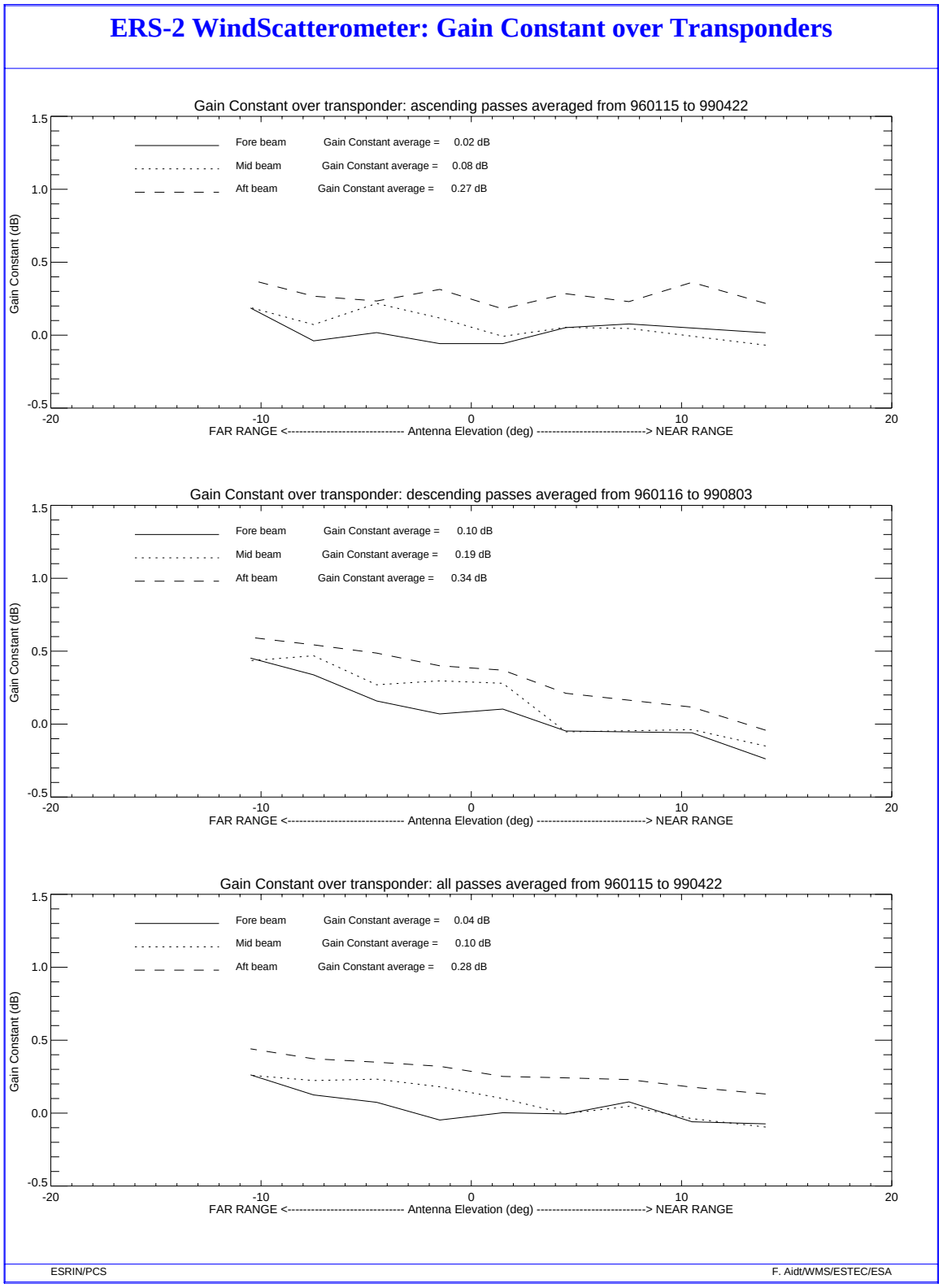


**FIGURE 4. ERS-2 Scatterometer: gain constant over transponders plus a scaling factor. All data available since January 1996. Upper plot: ascending passes. Middle plot: descending passes. Lower plot: all passes.**

## 2.2 Ocean Calibration

ECMWF performs the monitoring of ERS-2 sigma noughts over ocean (see the report in Annex).

The sigma nought bias is defined as the difference between the ERS-2 sigma-nought and the sigma nought retrieved using the CMOD-4 model with the First Guess at Appropriate Time (FGAT) background winds.

The sigma nought biases for the cycle 50 with respect to the ECMWF model first guess winds are similar to the results from the previous cycle. The impact of the new AOCS configuration on a large scale is negligible.

A special analysis of the sigma nought bias has been carried out in the region 55 - 45 degrees South. In this region as explained in section 3.1 the error in the satellite pointing is high (ascending passes only) and a change in the calibration is suspected. The Figure 4 (before the qualification period) and the Figure 5 (during the qualification period) show the result. The shape of the antenna pattern at descending passes show a good agreement between the qualification period and the pre-qualification. The only difference is in the error bar amplitude that is due to a different percentage of entries used. The result for the ascending passes is a clear change (close to 1 dB) in the shape of the antenna patterns in particular for the far range.

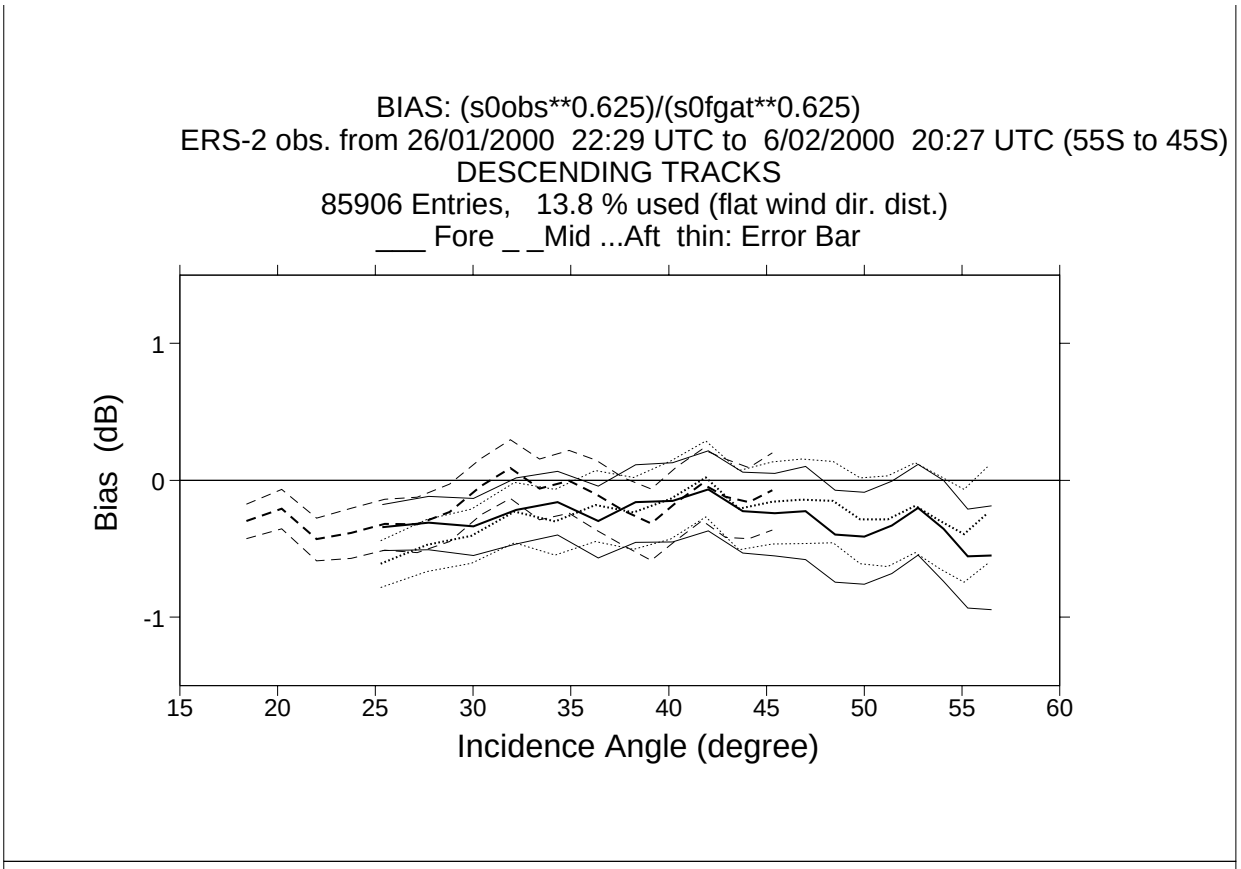


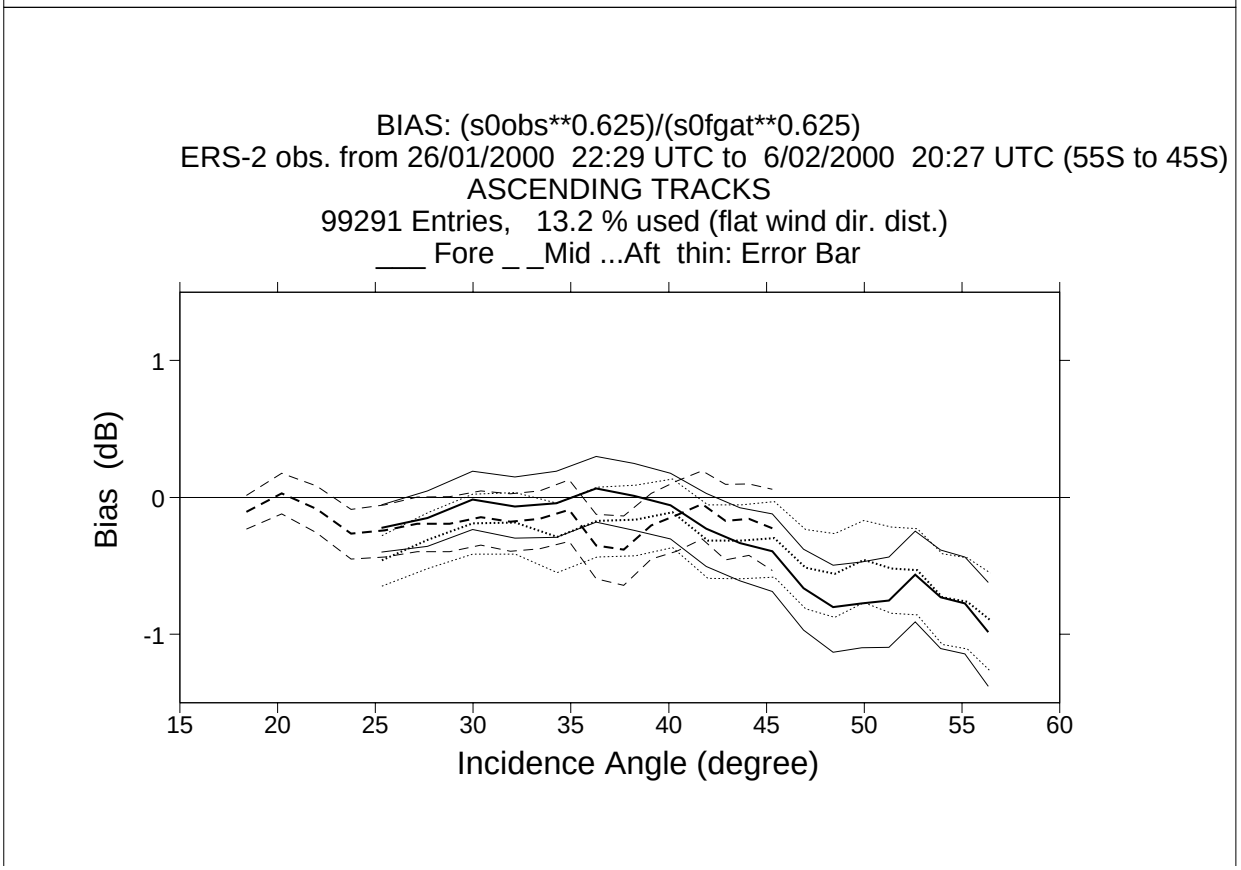


**FIGURE 5. ERS-2 Scatterometer: Ocean calibration (55-45 deg. South) before the qualification period**

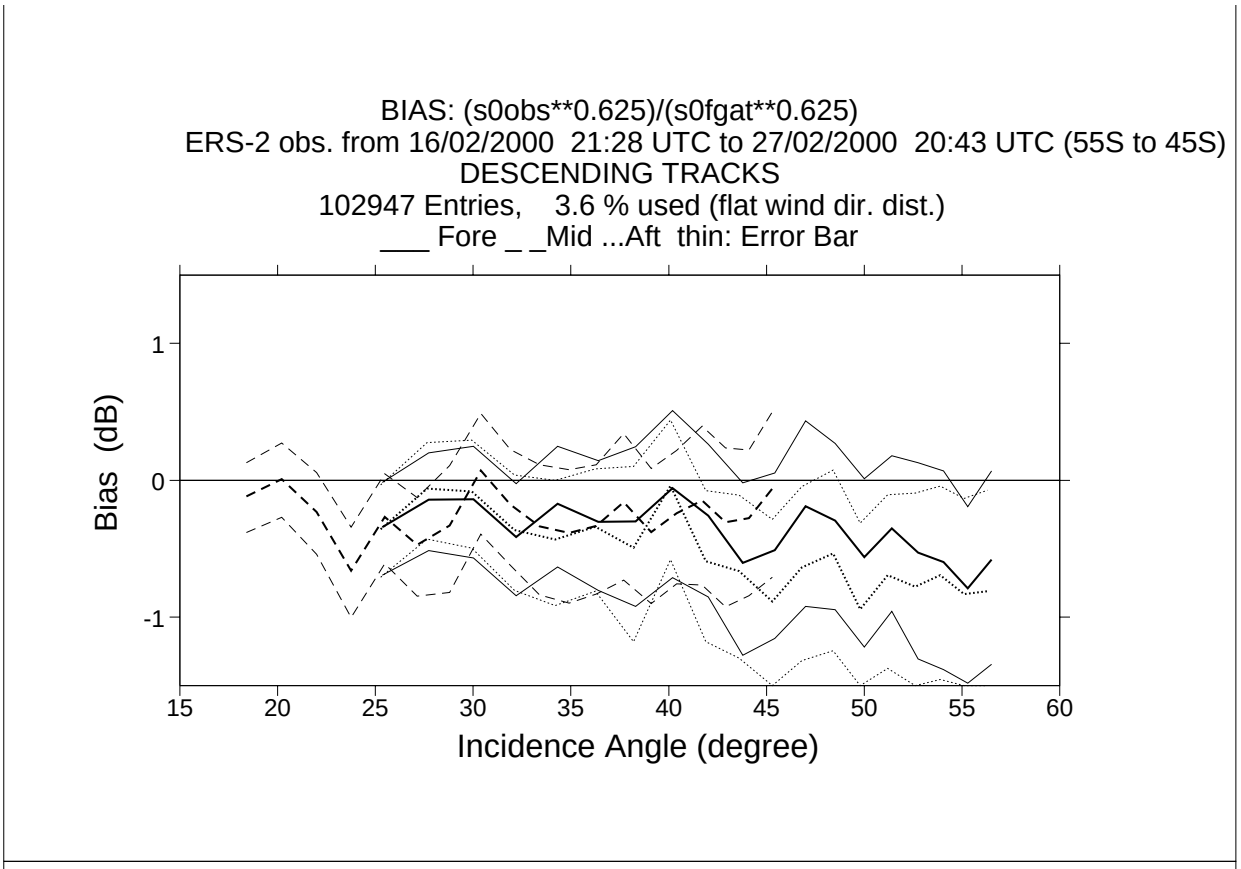


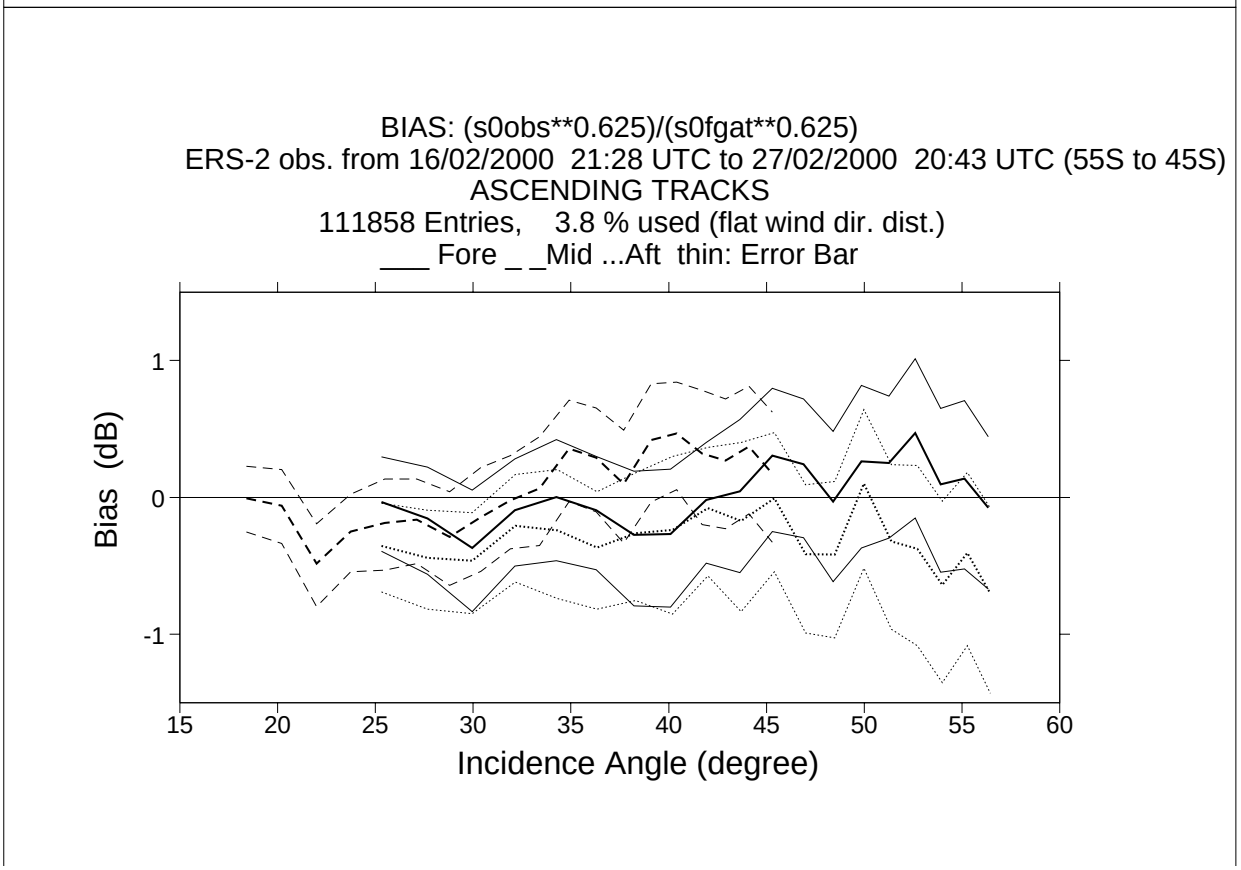


**FIGURE 6. ERS-2 Scatterometer: Ocean calibration (55-45 deg. South) qualification period**

## 2.3 Gamma-nought over Brazilian rain forest

Although the transponders give accurate measurements of the antenna attenuation at particular points of the antenna pattern, they are not adequate for fine tuning across all incidence angles, as there are simply not enough samples. The tropical rain forest in South America has been used as a reference distributed target. The target at the working frequency (C-band) of ERS-2 Scatterometer acts as a very rough surface, and the transmitted signal is equally scattered in all directions (the target is assumed to follow the isotropic approximation). Consequently, for the angle of incidence used by ERS-2 Scatterometer, the normalised backscattering coefficient (sigma-nought) will depend solely on the surface effectively seen by the instrument:

$$S^0 = S \bullet \cos\theta$$

With this hypothesis it is possible to define the following formula:

$$\gamma^0 = \frac{\sigma^0}{\cos\theta}$$

Using this relation, the gamma-nought backscattering coefficient over the rain forest is independent of the incident angle, allowing the measurements from each of the three beams to be compared.

The test area used by the PCS is located between 2.5 degrees North and 5.0 degrees South in latitude and 60.5 degrees West and 70.0 degrees West in longitude.

The following paragraphs give a description of the activities carried out with this natural target.

### 2.3.1 Antenna pattern: Gamma-nought as a function of elevation angle

This analysis is carried out by ESTEC that has selected a larger region than the one used as test area within PCS. In this case the selected rain forest extends from 2.0 degrees South to 11.0 degrees South in latitude and 56.0 degrees West to 80 degrees West in longitude. A large area is selected in order to have a larger amount of measurements.

For cycle 50 the antenna patterns as function of the elevation angle have not been computed by ESTEC.

### 2.3.2 Antenna pattern: Gamma-nought as a function of incident angle

Figure 7 shows the antenna patterns as a function of the incident angle for cycle 50.

The antenna patterns for the cycle 50 are very close to the ones obtained in the previous cycle. The antenna patterns show a flat profile, within 0.3 dB for the descending passes and within 0.4dB for the ascending ones with a small slope at the near range.

The mid antenna profile is roughly 0.1 dB less than the fore and aft ones (in particular for the descending passes).

Special investigation has been done to check the impact of the new AOCS configuration on the antenna patterns. The Figures 8,9, 10 and 11 show the antenna patterns computed for the relative tracks from 267 to 496 during the years 1997, 1998, 1999 and 2000 respectively. The antenna profiles computed during the qualification period are very similar to the ones obtained in the previous years. Small difference are within the variability of the test area. The bias in the level from 1997 to 1998 onwards is due to the new calibration setting in the ground processing.

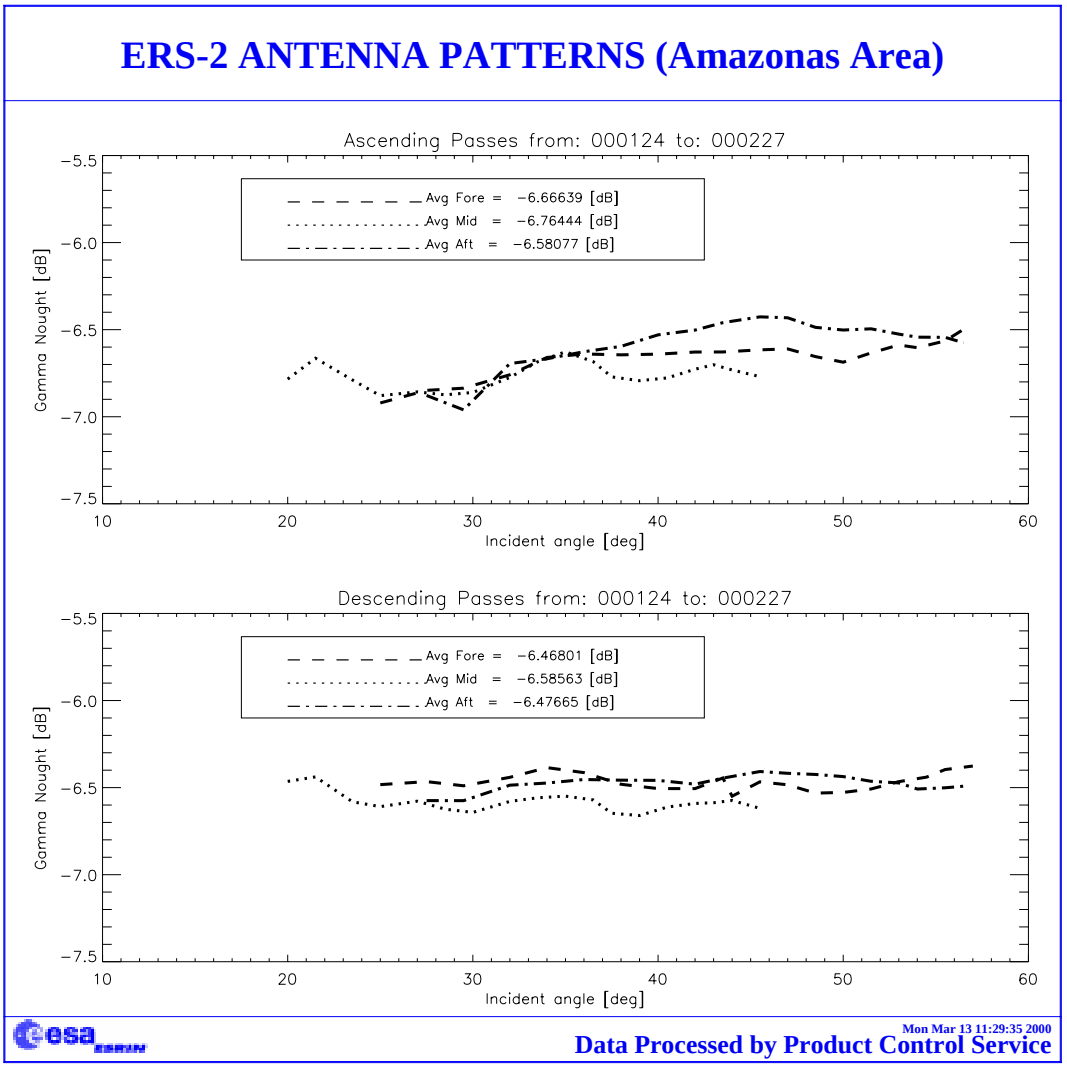


**FIGURE 7. ERS-2 Scatterometer antenna patterns as function of the incident angle: cycle 50.**

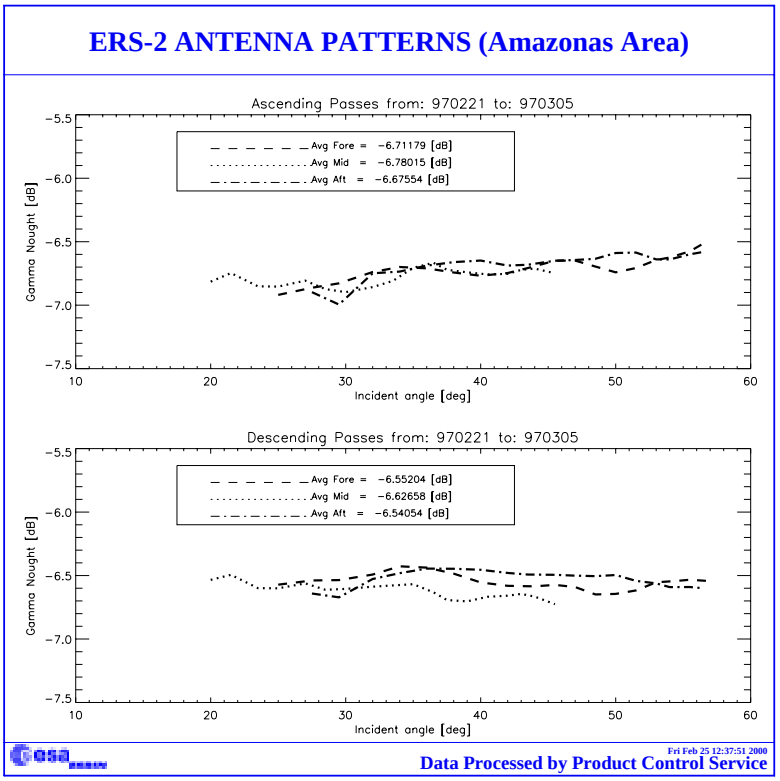


**FIGURE 8. Antenna pattern relative track from 267 to 496 year 1997**

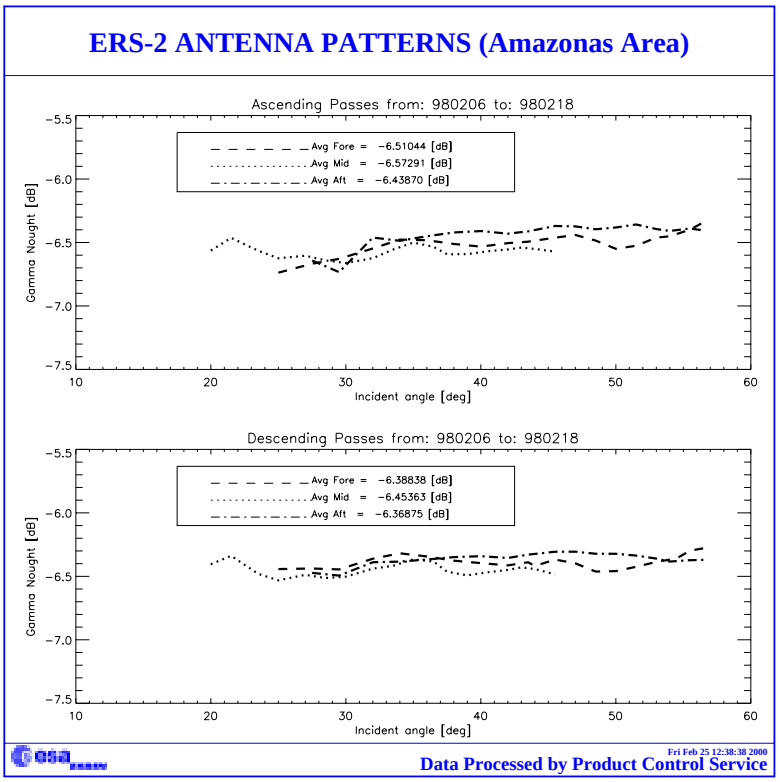


**FIGURE 9. Antenna pattern relative track from 267 to 496 year 1998**

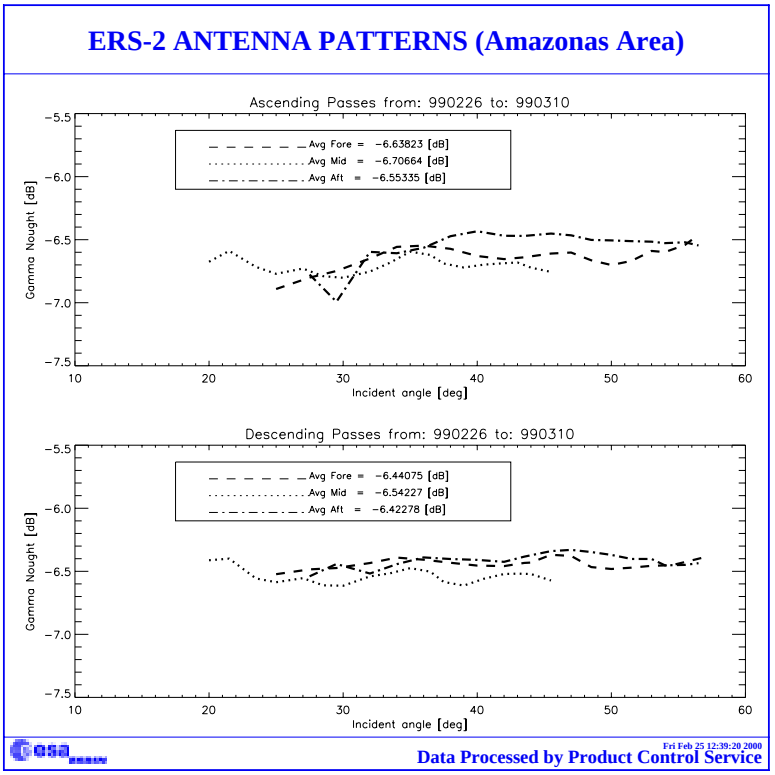


**FIGURE 10. Antenna pattern relative track from 267 to 496 year 1999**

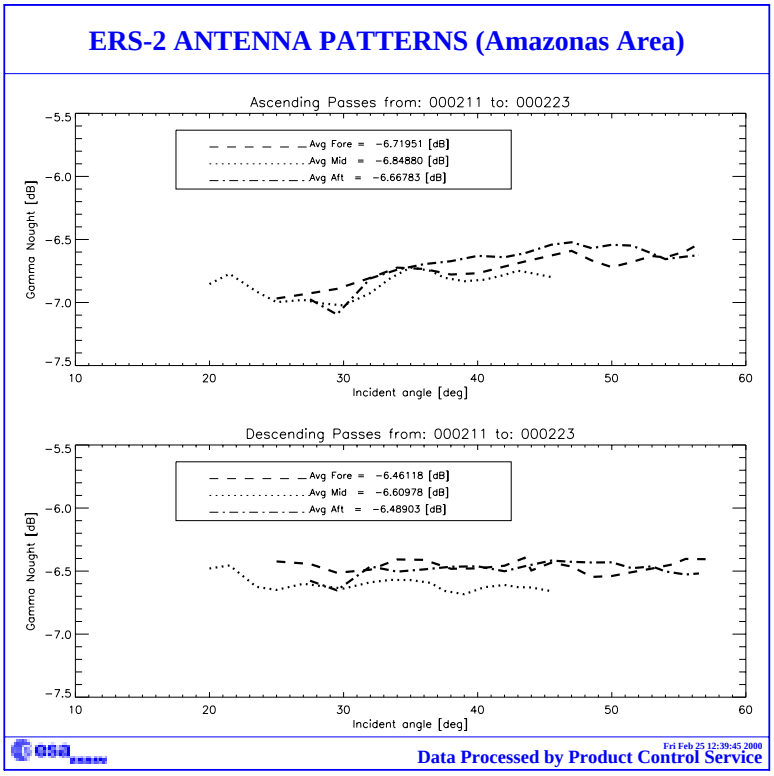


**FIGURE 11. Antenna pattern relative track from 267 to 496 year 2000.**

### 2.3.3 Gamma-nought histograms and peak position evolution

As the gamma-nought is independent from the incidence angle, the histogram of gamma-noughts over the rain forest is characterised by a sharp peak. The time-series of the peak position gives some information on the stability of the calibration. This parameter is computed by fitting the histogram with a normal distribution added to a second order polynomial:

$$F\langle x\rangle = A_0 \cdot \exp\left(-\frac{z^2}{2}\right) + A_3 + A_4 \cdot x + A_5 \cdot x^2$$

where: $z = \dfrac{x - A_1}{A_2}$

The parameters are computed using a non linear least square method called “gradient expansion”. The position of the peak is given by the maximum of the function F(x). The histograms are computed weekly (from Monday to Sunday) for each antenna individually (“Fore”, “Mid”, and “Aft”) and for ascending and descending passage with a bin size of 0.02 dB.

Figure 12 shows the evolution of the histograms peak position since January 1996. The step shown in March 1996 is due to the end of commissioning phase when a new Look Up Table was used in the ground stations for WSCATT FD-products generation. It is interesting to note the decrease of roughly 0.2 dB from August 1996 to June 1997. This is linked to the switch of the Scatterometer calibration subsystem from side A to side B on 6th of August. The redundancy of side A device caused a little change in the calibration that was corrected on 19$^{th}$ June 1997 with a new calibration LUT used in the ground processing.

Figure 13 shows the evolution of the peak position corrected with the new calibration set also for the period from August 1996 to June 1997. From the plots in figure 13 it is clear that the calibration stability achieved over the rain forest is within 0.5 dB. A seasonal effect is also present in the peak position evolution for the three antennae.

For the inter-beam calibration the results are shown in Figure 14. On average the peak values for the aft and fore antenna are very close together. The difference between the fore antenna signal and the mid antenna signal is roughly 0.1 dB (both ascending and descending passes) while the difference between the aft antenna signal and the mid antenna signal seems to have a seasonal behaviour. This differences is close to 0.1 dB during the summer and it is close to 0.2 dB during the winter for the ascending passes. For the descending passes the differences between the winter and the summer is less clear and the aft-mid inter-beam calibration is around 0.15 dB.

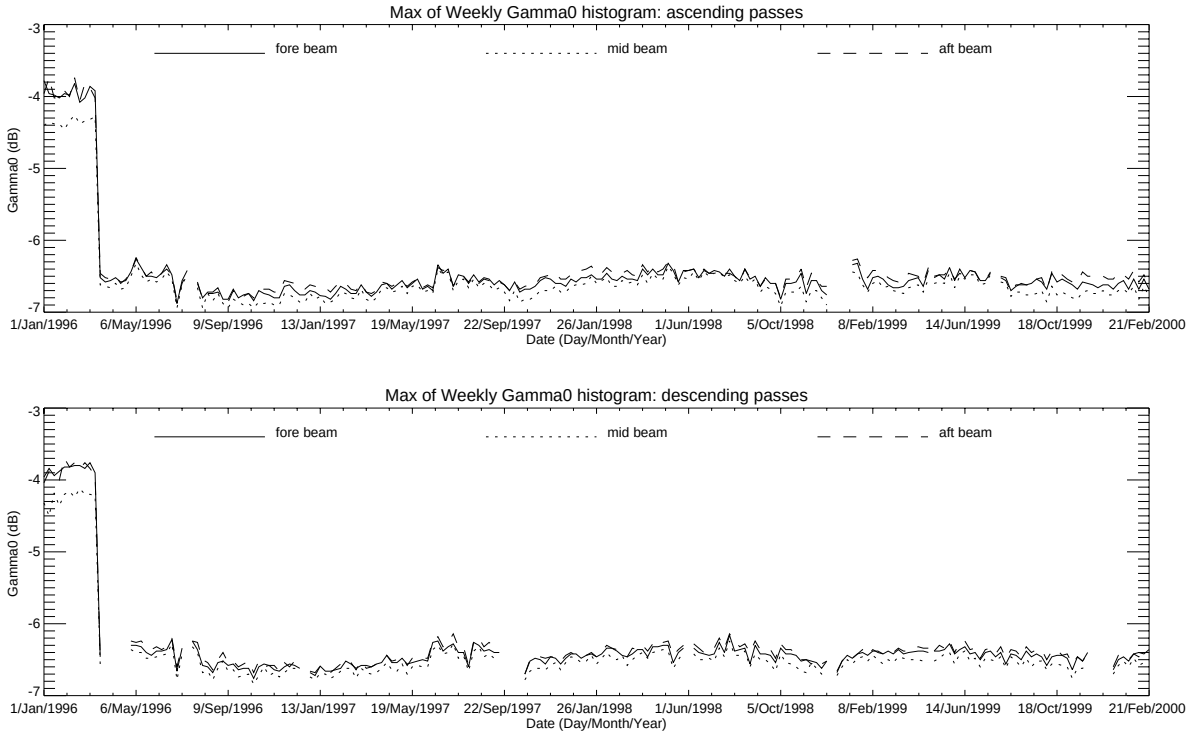


**FIGURE 12. ERS-2 Scatterometer, gamma-nought histogram: weekly evolution of maximum position. From up to down: ascending passes, descending passes.**

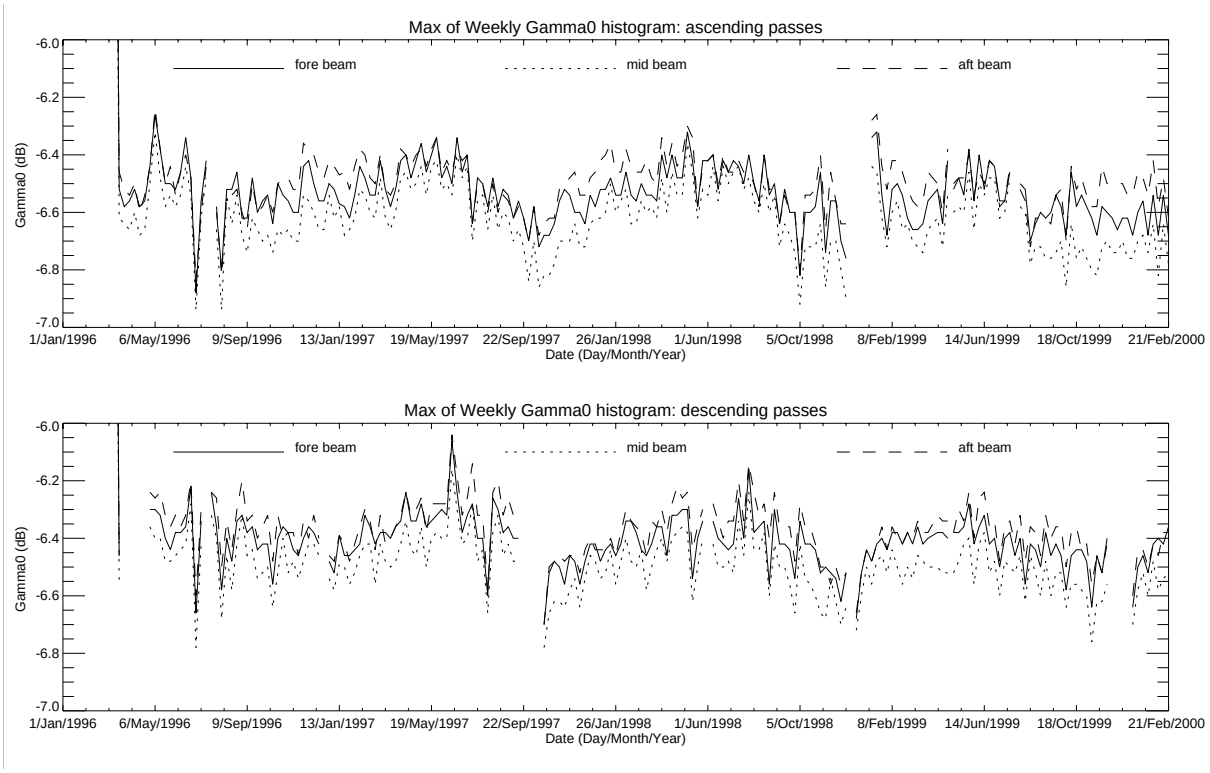


**FIGURE 13. Gamma-nought histogram: weekly evolution of maximum position. Data from 6th of August 1996 to 19th June 1997 are corrected with the new calibration constant (+0.2dB). Upper plot: ascending passes. Lower plot: descending passes.**

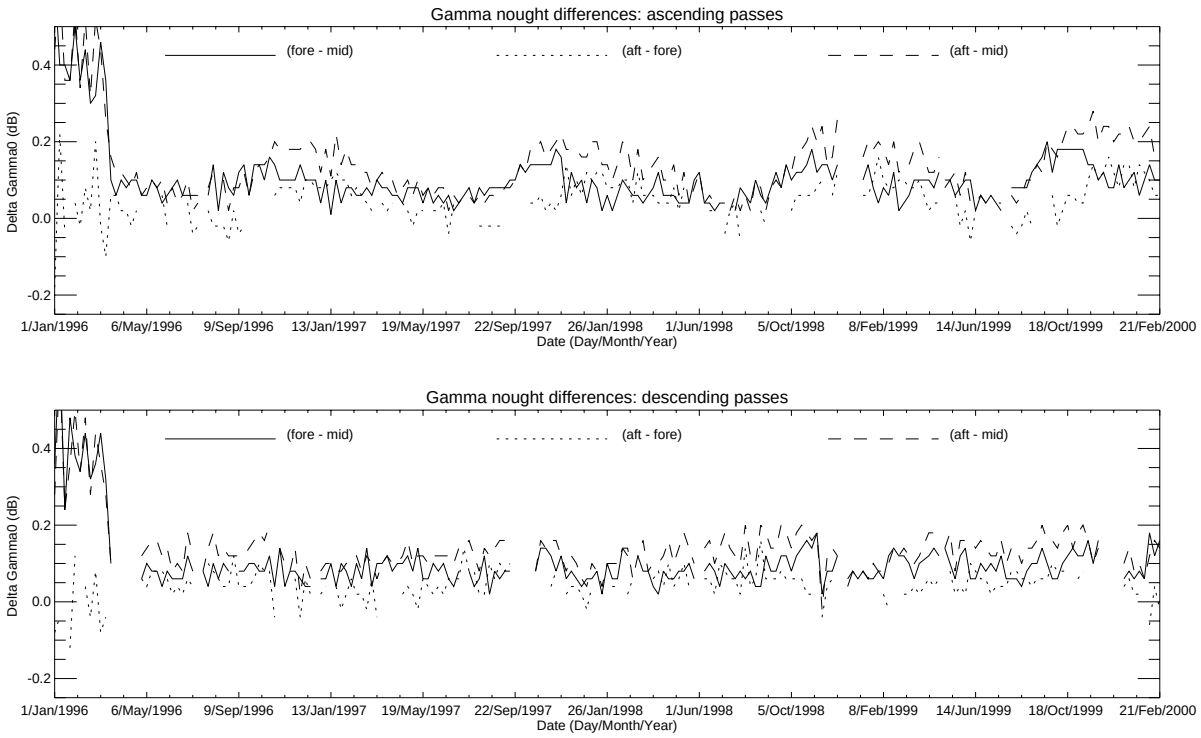


**FIGURE 14. inter-beam calibration, weekly differences of the maximum position. From up to down: ascending passes, descending passes.**

The mean and the standard deviation of gamma-nought are weekly computed directly using the Fast Delivery data. Figure 15 shows the evolution of the standard deviation since September 1996. The ascending passes show a gamma nought standard deviation more higher than the descending ones. This can be explained because at ascending passes the test site appears less homogeneous in particular for some areas near the rivers (see Figure 21). The last plot in Figure 15 shows the number of valid measurements used to compute the statistics. It is clear the reduction of the number of valid observation since the beginning of 1999. This is due to an increase of SAR images acquired over the Amazon rain forest.

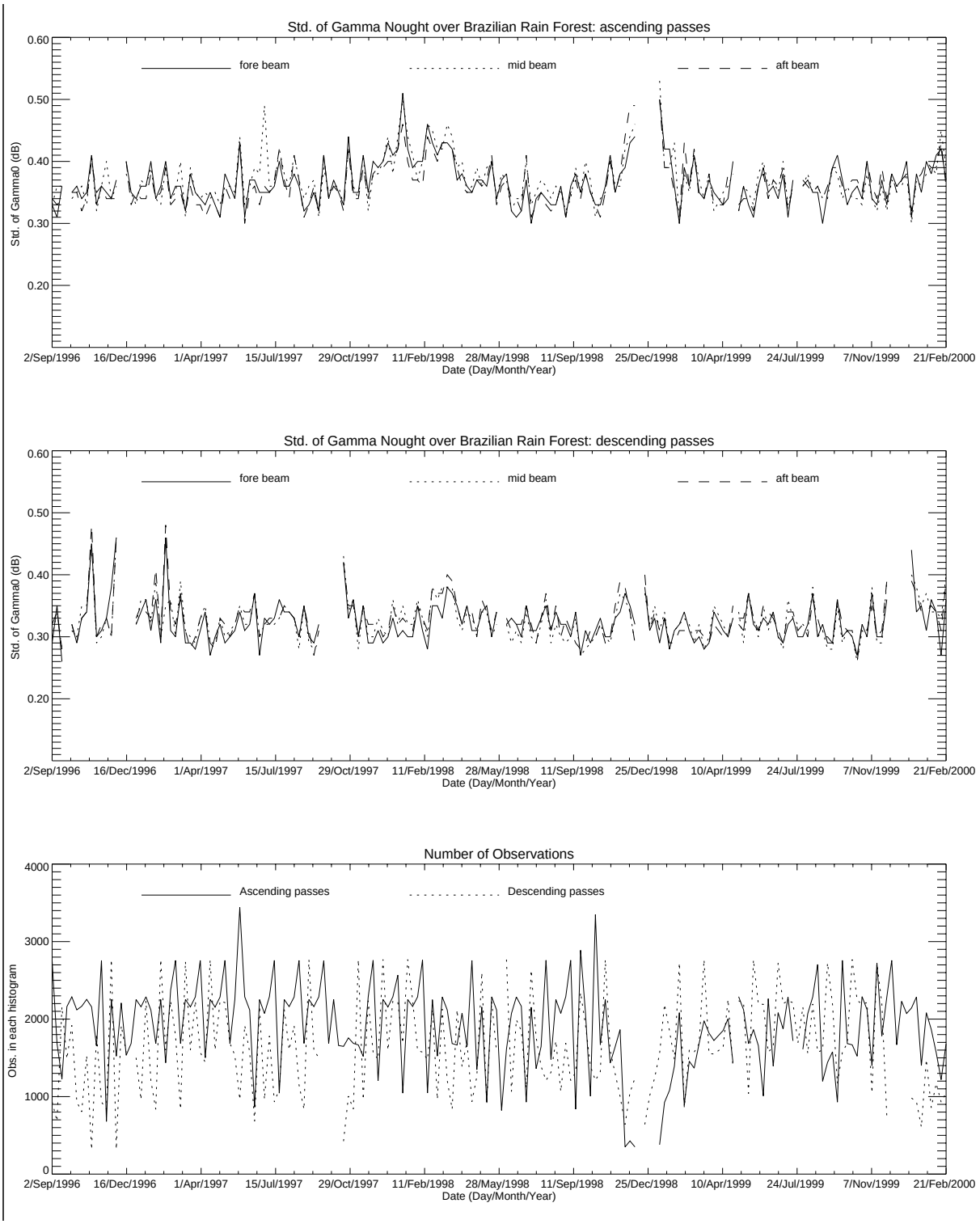


**FIGURE 15. Gamma-nought histograms: weekly evolution of standard deviation. From up to down: ascending passes standard deviation, descending passes standard deviation, number of valid observations.**

The Figures from 16 to 20 show the gamma-nought histogram over the Brazilian rain forest throughout cycle 50.

The shape of the weekly histograms shows slightly noise, the position of the maximum is within the nominal range.

The Figure 21 shows the gamma nought histogram during the qualification period (14 days). The position of the maximum, is very close to the one computed for the same relative tracks during the years 1999, 1998 and 1997 (see Figure 22,23, and 24) and the small difference are within the variability of the rain forest. The shape of the histograms computed during the qualification period is slightly more noisy in particular for the ascending passes. This confirm the behaviour noted in the weekly histograms but we need more observation to conclude that the small change in the histogram' s shape is due to the new AOCS configuration or it is a geophysical effect (see Figure 25).

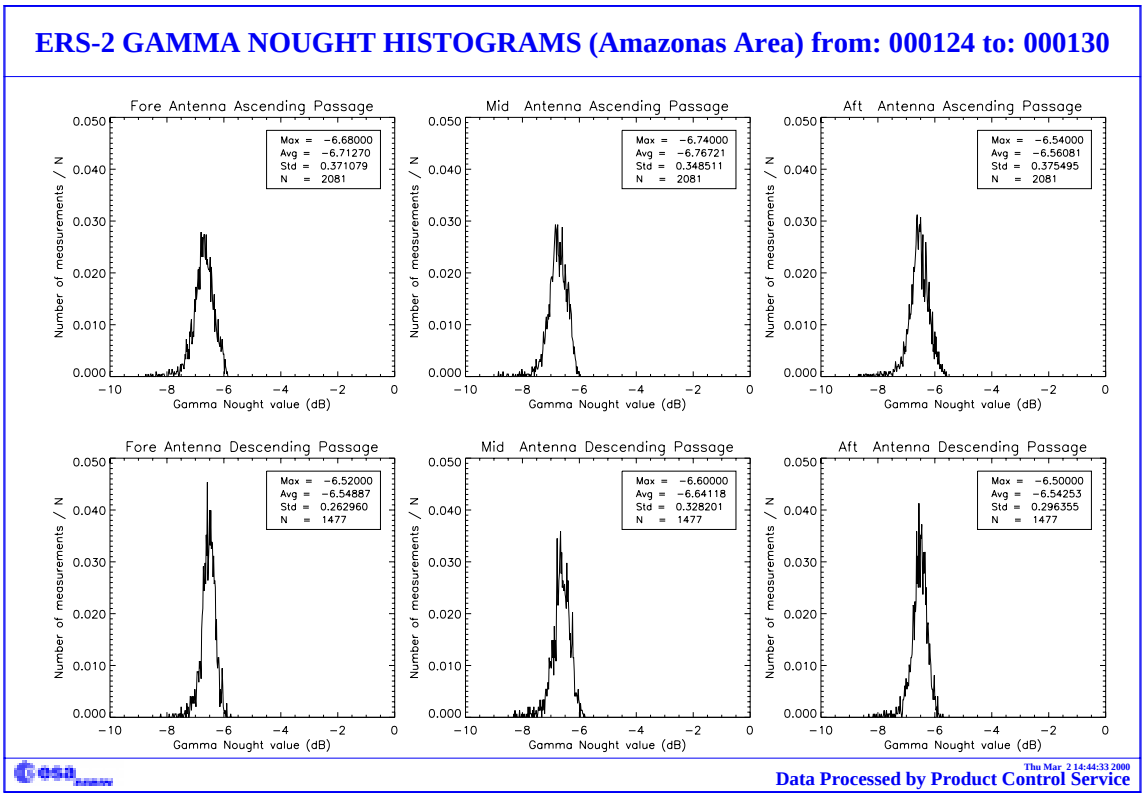


**FIGURE 16. Gamma-nought histograms over Brazilian Rain forest: first week of the cycle 50**

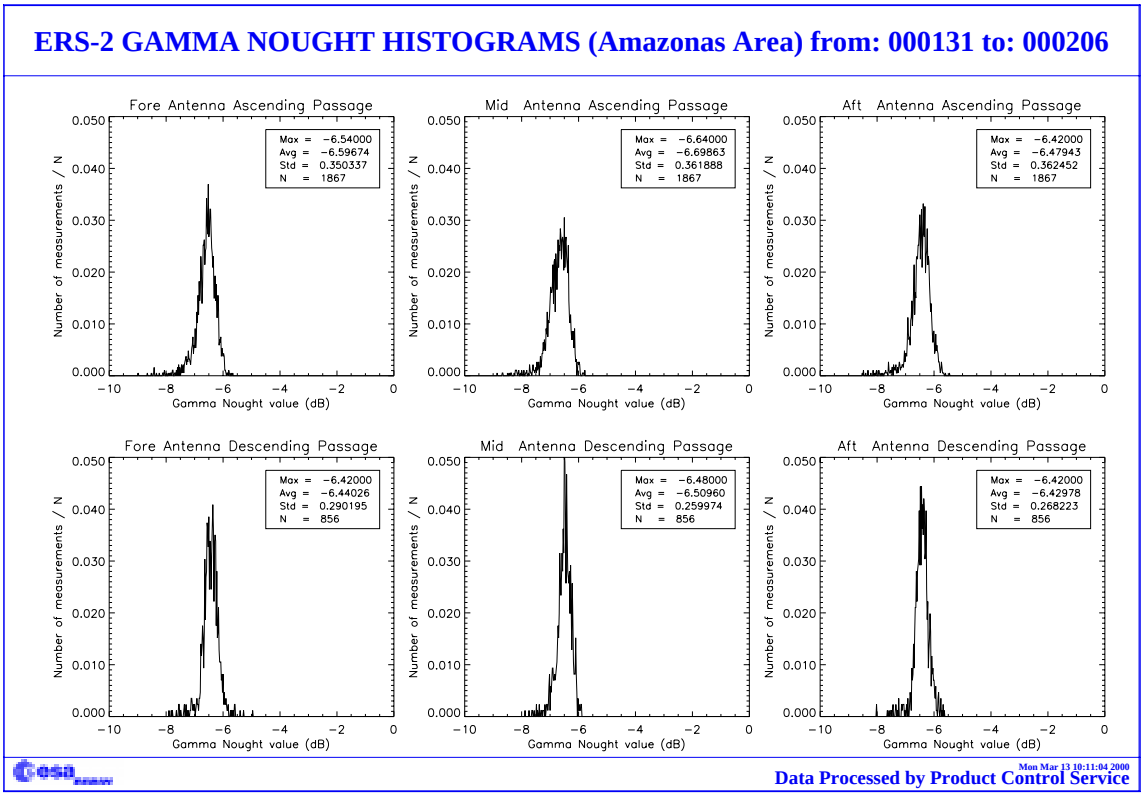


**FIGURE 17. Gamma-nought histograms over Brazilian Rain forest: second week of the cycle 50**

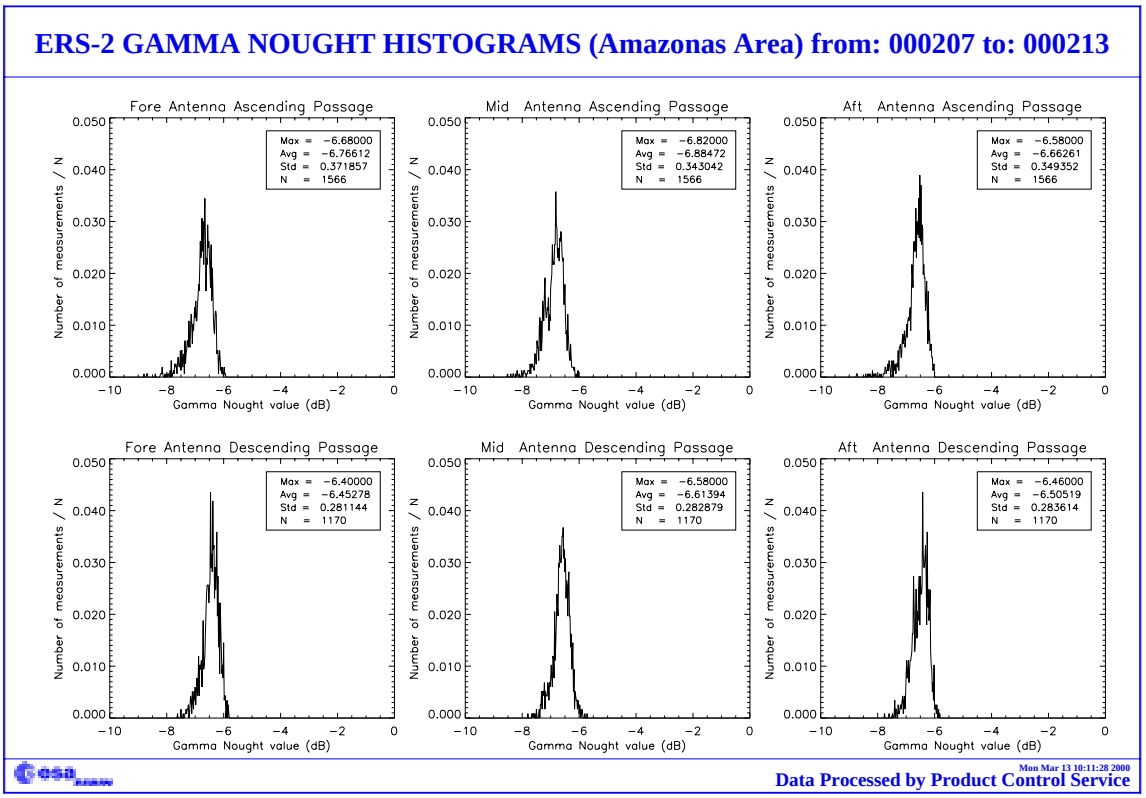


**FIGURE 18. Gamma-nought histograms over Brazilian rain forest: third week of the cycle 50**

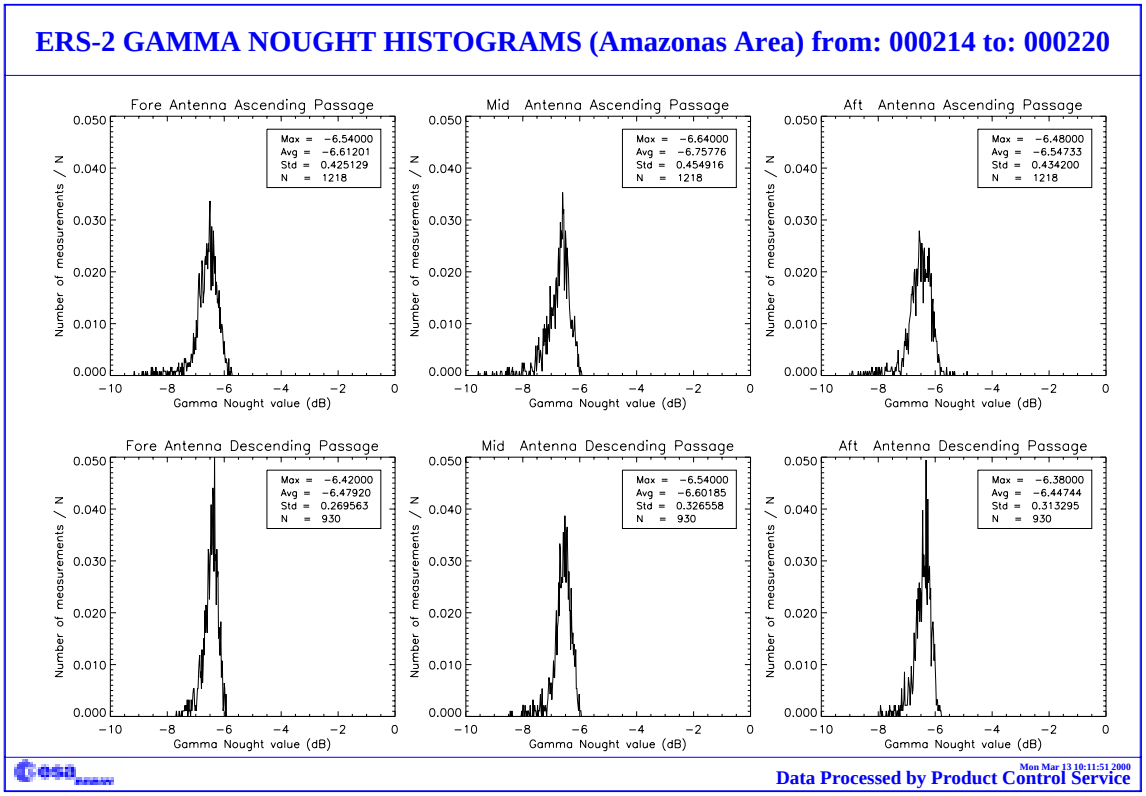


**FIGURE 19. Gamma-nought histograms over Brazilian rain forest: fourth week of the cycle 50.**

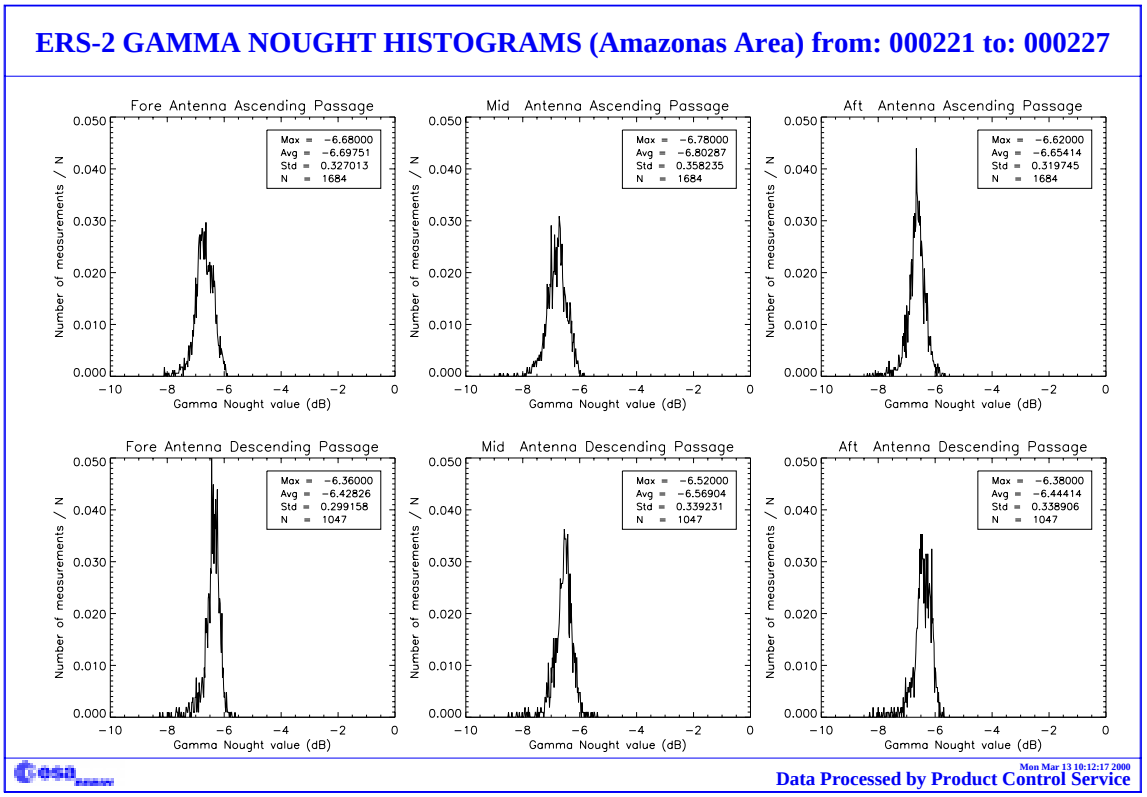


**FIGURE 20. Gamma-nought histograms over Brazilian rain forest: fifth week of the cycle 50.**

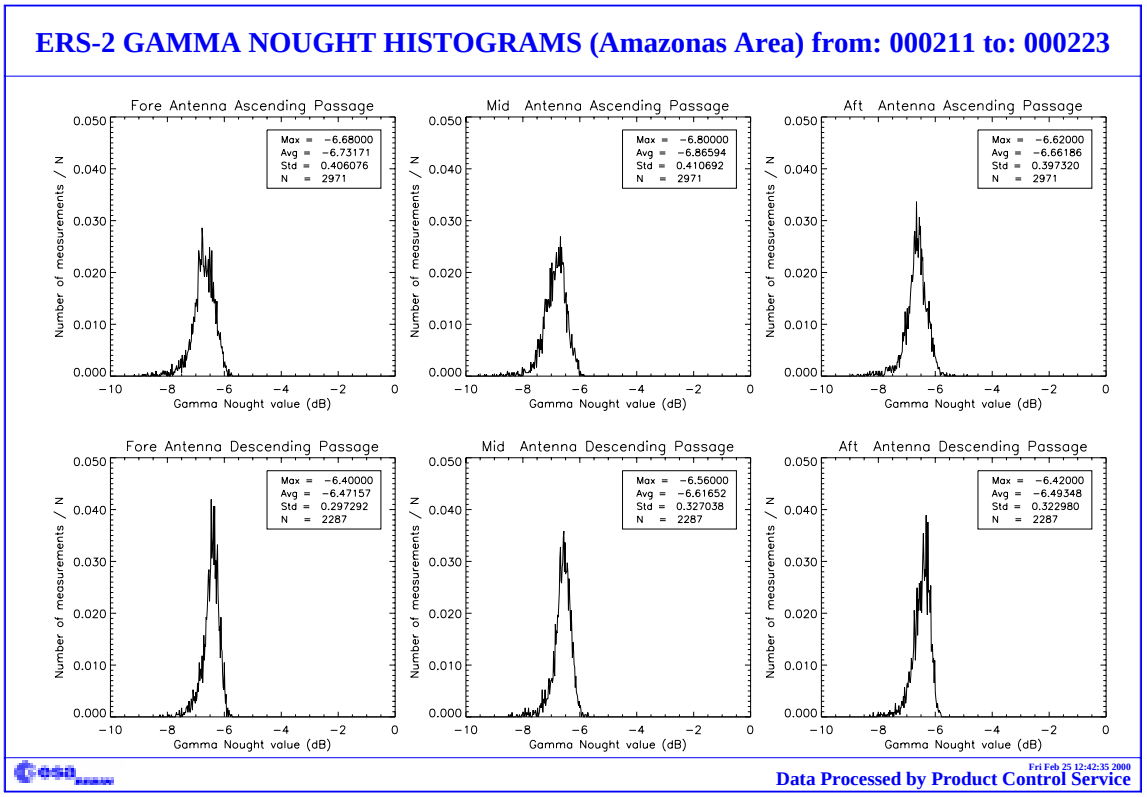


**FIGURE 21. Gamma nought histograms from 11th February 2000 to 23rd February 2000 during the qualification period (relative tracks from 267 to 469).**

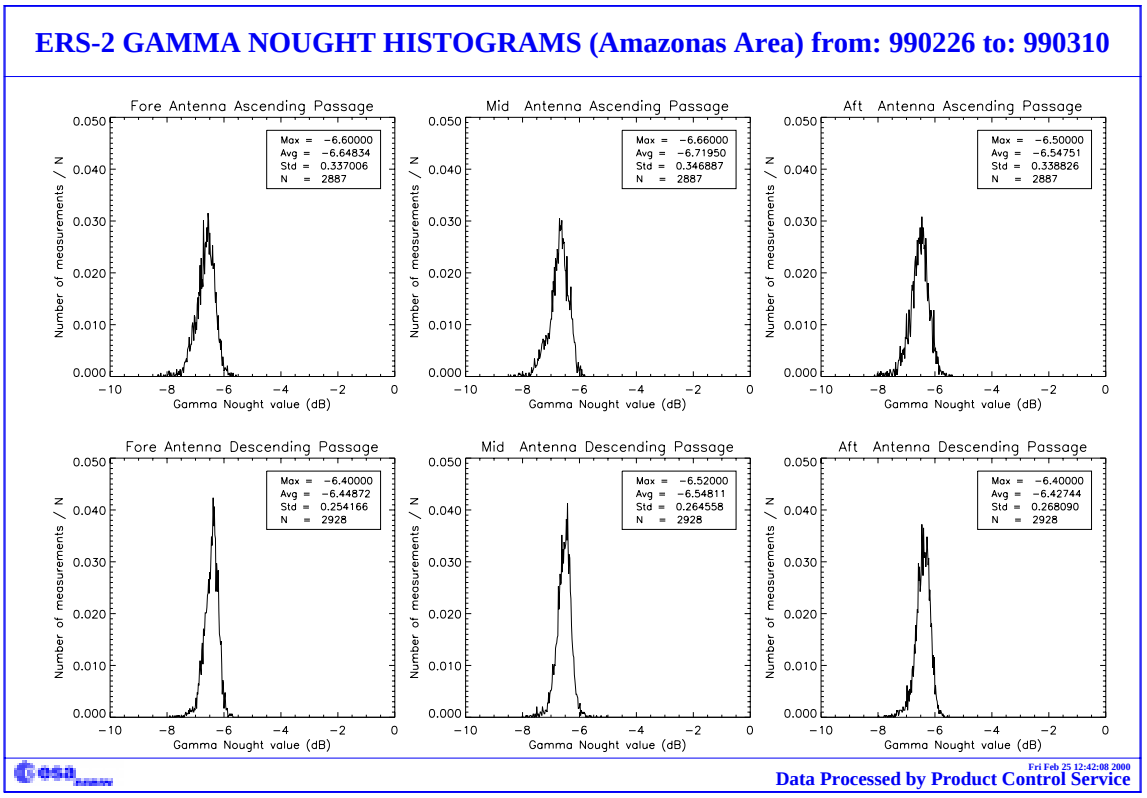


**FIGURE 22. Gamma nought histograms relative tracks from 267 to 496 year 1999**

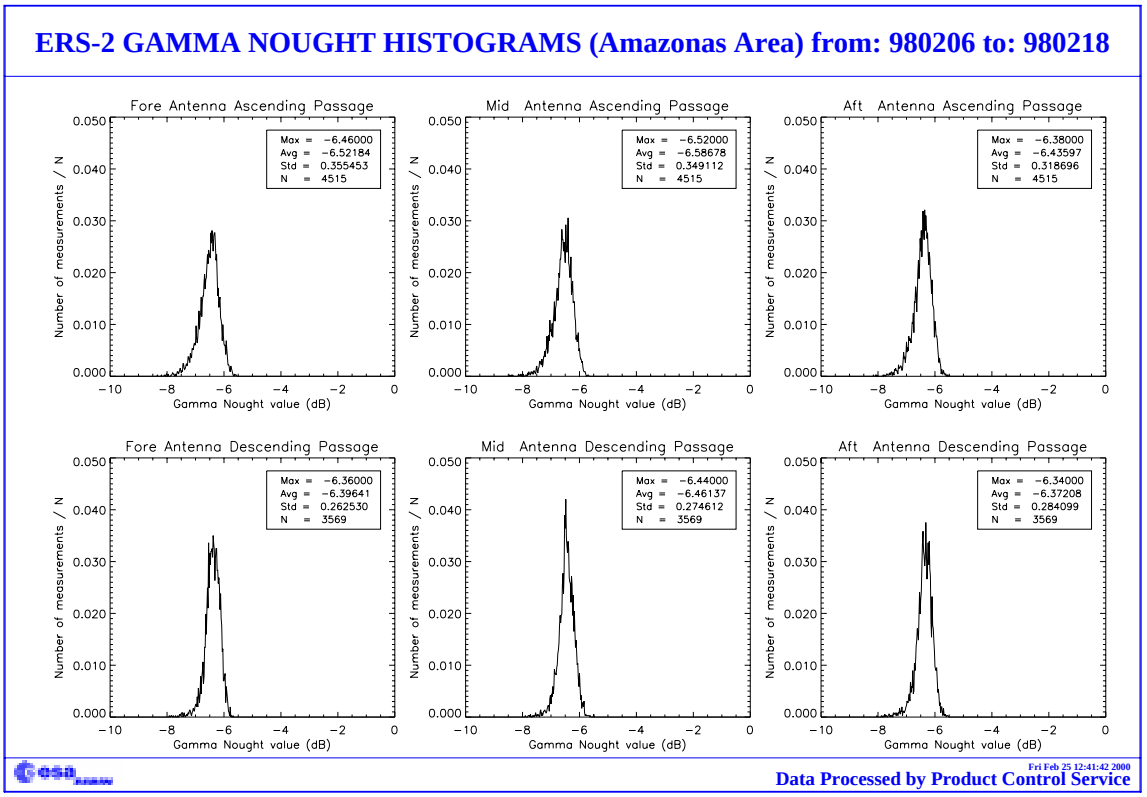


**FIGURE 23. Gamma nought histograms relative tracks from 267 to 496 year 1998**

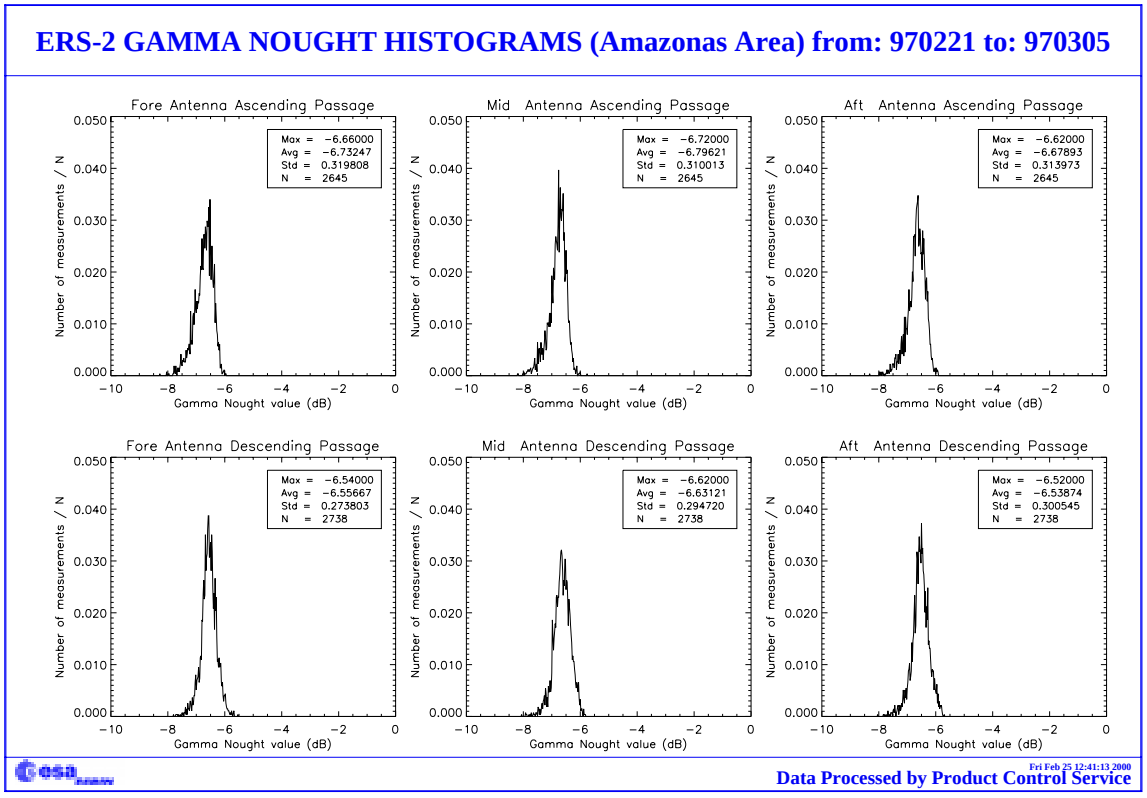


**FIGURE 24. Gamma nought histogram relative tracks from 267 to 496 year 1997**

### 2.3.4 Gamma nought image of the reference area

The Figure 25 shows maps of the gamma nought over the Brazilian rain forest. This is the area where statistics are computed.

Each map has a resolution of 0.5 degrees in latitude and 0.5 degrees in longitude, roughly this is the instrument resolution at the latitude of the test site. In each resolution cell falls the average of all the valid observations available during one cycle (35 days).

From the figures no important changes happened in the test area during the cycle 50. As outlined in the previous reports the test area appears less homogenous at the ascending passes than in the descending ones. This seems due to the signal that comes from some areas near the rivers.These areas make the gamma nought histogram more noisy at ascending passes rather than at descending passes.

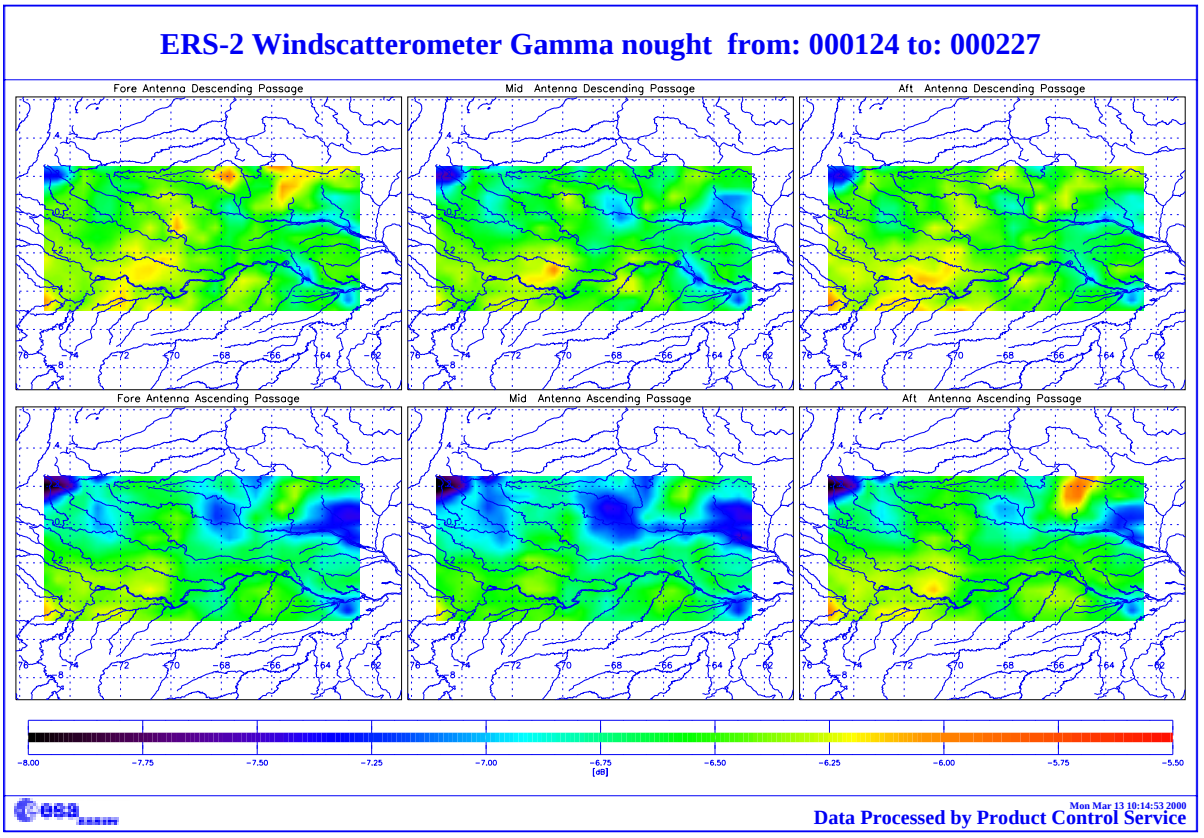


**FIGURE 25. ERS-2 Scatterometer: gamma nought over the Brazilian rain forest cycle 50.**

### 2.3.5 Sigma nought evolution

The Figures 26 and 27 show the evolution of the sigma nought (mid beam) over the reference area. The analysis is done per orbit and per node and the scope is to evaluate the impact of the new mono-gyro software on the sigma nought. The relative track chosen are those where the number of valid measurements for each node is greater than 20.

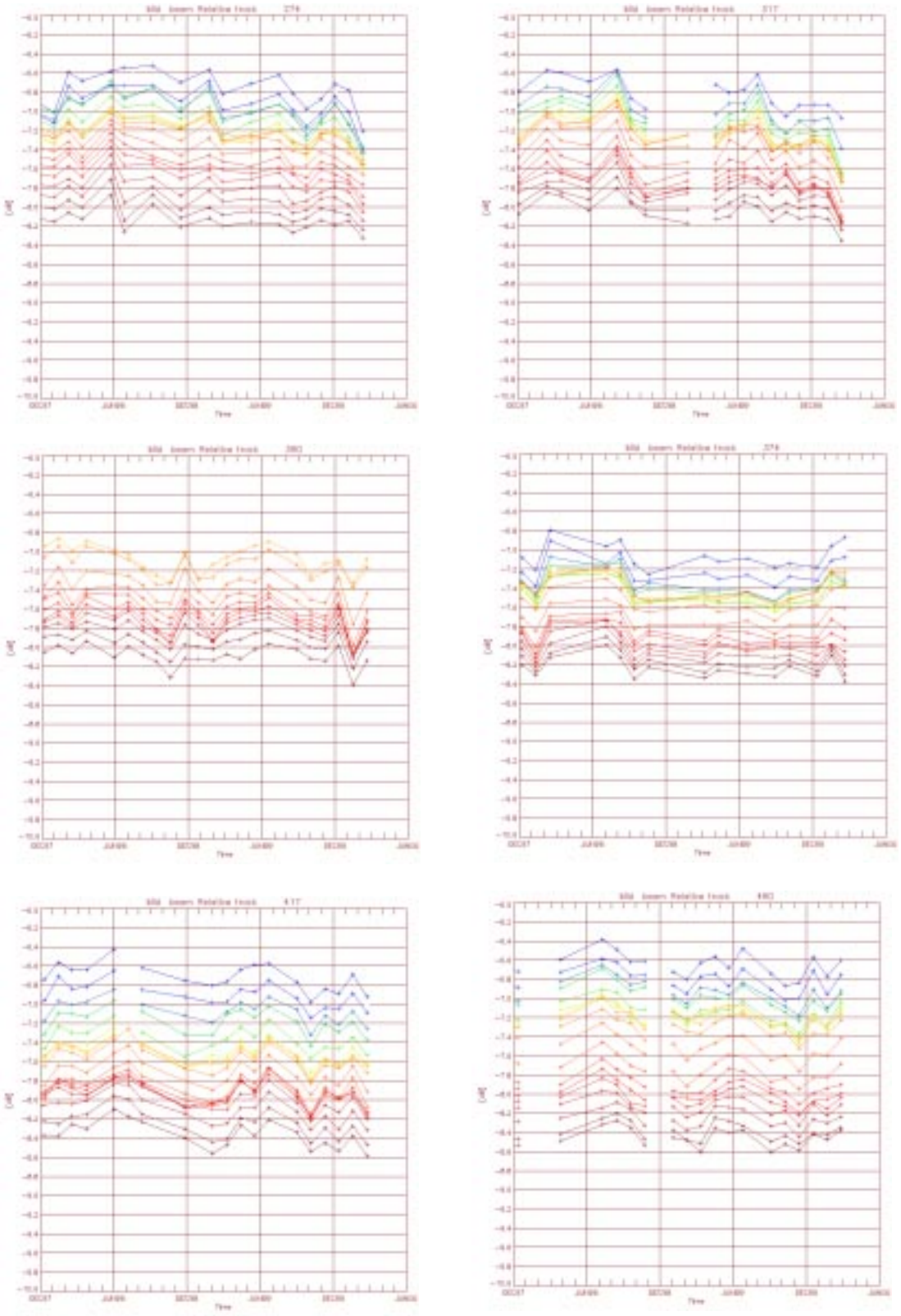

**FIGURE 26. Sigma nought ascending passes mid beam (since December 1997)**

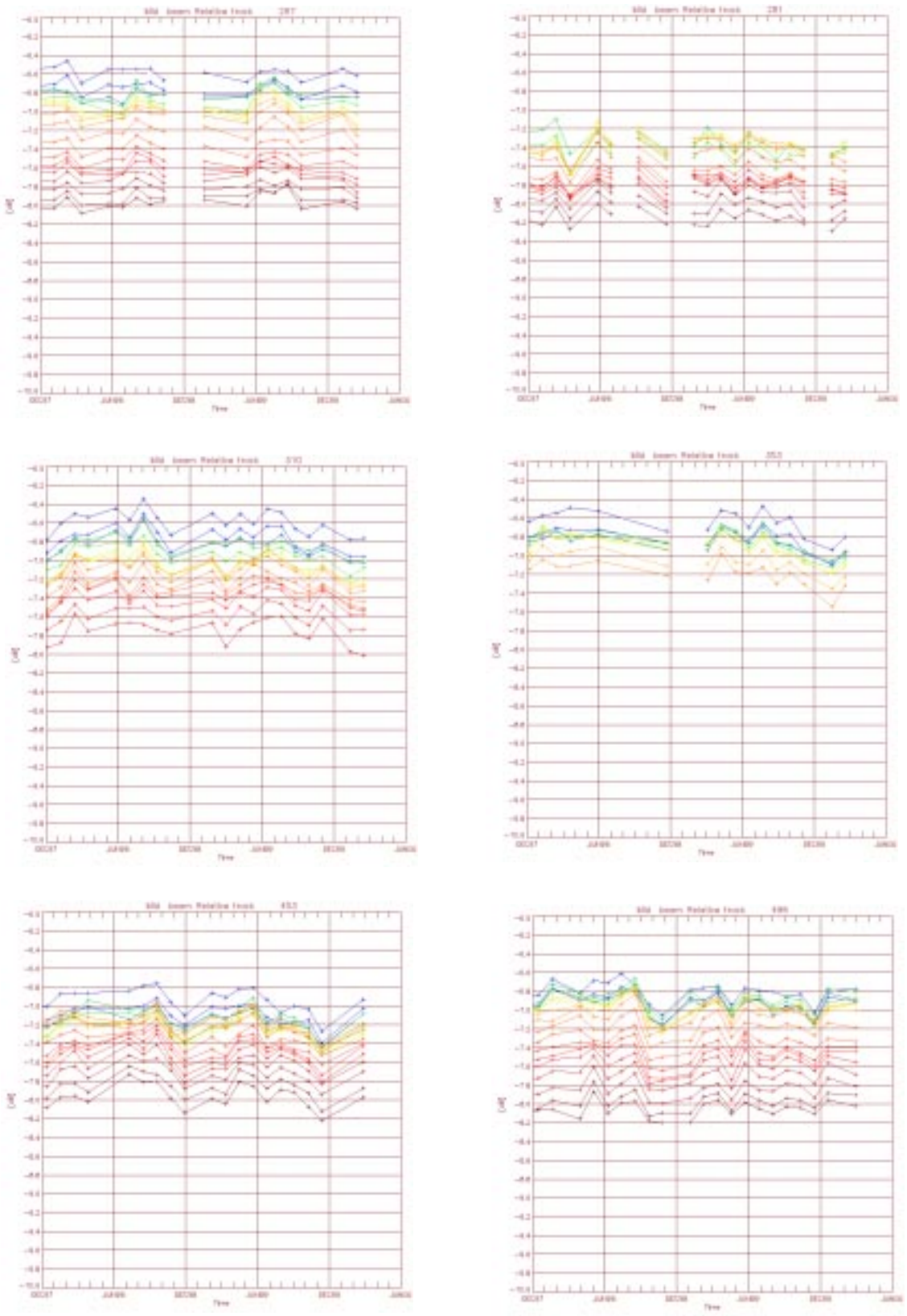

**FIGURE 27. Sigma nought descending passes mid beam (since December 1997)**

The time series show that during the qualification period (the last two measurements in the plots) the descending passes signal has been more stable than the ascending passes signal. However from these data it is not clear an impact of the new AOCS configuration in the sigma nought level.

### 2.3.6 Antenna temperature evolution over the Rain Forest

The monitoring of the antenna temperature over the Brazilian rain forest is performed by PCS. The antenna temperatures are retrieved from the satellite telemetry when the Scatterometer swath is over the test site and the instrument is active (AMI in wind only or wind/wave mode). The scope of this monitoring is to investigate a possible correlation between the antenna temperatures and the gamma-nought level. This correlation is not clear in the actual data because of the gamma nought variability of the selected area. A deep analysis is to be performed to better understand the facts.

The plots for the three beams and for the ascending, descending and all passes are in Figure 28. It is interesting to note that the annual variation is due to the earth inclination and that the antenna temperatures have an increase of roughly 1.0 degree per year in the case of the mid and fore antenna; 2 degrees per year for the aft antenna.

This temperature increase could be related to the degradation of the antennae protection film.

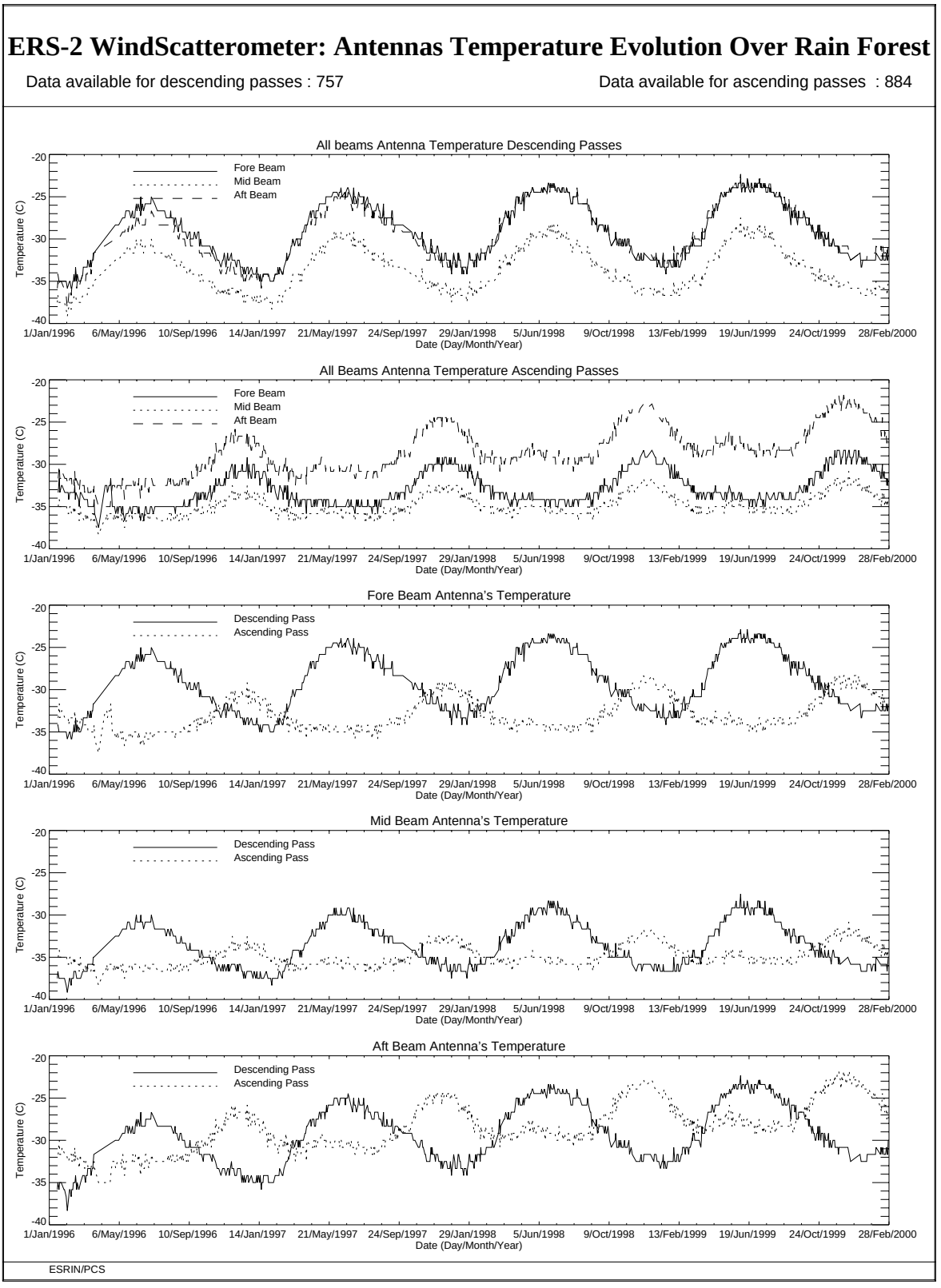


**FIGURE 28. ERS-2 Scatterometer: evolution of the antenna temperatures over the Brazilian rain forest.**

# 3.0 Instrument performance

The instrument status is checked by monitoring the following parameters:

- Centre of Gravity (CoG) and standard deviation of the received signal spectrum. This parameter is useful for the monitoring of the orbit stability, the performances of the doppler compensation filter, the behaviour of the yaw steering mode and the performances of the devices in charge for the satellite attitude (e.g. gyroscopes, earth sensor).
- Noise power I and Q channel.
- Internal calibration pulse power.

the latter is an important parameter to monitor the transmitter and receiver chain, the evolution of pulse generator, the High Power Amplifier (HPA), the Travelling Wave Tube (TWT) and the receiver.

These parameters are extracted daily from the UWI products and averaged. The evolution of each parameter is characterised by a least square line fit. The coefficients of the line fit are printed in each plot.

## 3.1 Centre of gravity and standard deviation of received power spectrum

The Figure 29 shows the evolution of the two parameters for each beam.

The tendency from the beginning of the mission to the operation with the new Attitude On-board Control System (AOCS) configuration (7$^{th}$ February 2000) is a clear and regular increase of the Centre of gravity (CoG) for the three antennae. After the 7$^{th}$ February 2000 the CoG shows an increase of roughly 200 Hz due to the new AOCS.

The old AOCS configuration (one Digital Earth Sensor - DES, one Digital Sun Sensor - DSS and 3 gyros) is no more considered safe because 3 of the six gyros on-board are out of order or very noisy. The new attitude control configuration is designed to pilot the ERS-2 using only one gyro plus the DES and the DSS modules. Scope of this new configuration is to extend the satellite lifetime by using the available gyros one at the time.

The evolution of the CoG standard deviation is more stable apart from the change occurred on 26$^{th}$, October 1998. On October 26$^{th}$, 1998 the standard deviation of the CoG had, on average, a decrease of roughly 100 Hz for the fore and aft antenna and of roughly 30Hz for the mid antenna. This change is linked with the increase of the transmitted power (see 3.3).

Others changes in the AOCS configuration are recognised in Figure 29. The two steps observed at the beginning of the plots of the CoG (see Figure 28) are due to a change in the pointing subsystem (DES reconfiguration) side B instead of side A after a depointing anomaly (see table 2 for the list of the AOCS depointing anomaly occurred during the ERS-2 mission). The first change is from 24$^{th}$, January 1996 to 14$^{th}$, March 1996, the second one is from 14$^{th}$ February 1997 to 22$^{nd}$ April 1997. During these periods side B was switched on. It is important to note that during the first time a clear difference in the CoG is present only for the Fore antenna (an increase of roughly

100 Hz) while during the second time the change has affected all the three antennae (roughly an increase of 200 Hz, 50 Hz and 50 Hz for the fore, mid and aft antenna respectively).

**Table 2: ERS-2 Scatterometer AOCS depointing anomaly**

| From | To |
|---|---|
| 24th January 1996 9:10 a.m. | 26th January 1996 6:53 p.m |
| 14th February 1996 1:25 a.m. | 15th February 1996 3:44 p.m |
| 3rd June 1998 2:43 p.m. | 6th June 1998 12:47 a.m. |
| 1st September 1999 8:50 a.m. | 2nd September 1999 1:28 a.m. |

The Figure 29 shows also when the satellite was operated in Fine Pointing Mode (FPM) or the on-board doppler compensation was missing. These events are related with the large peaks in the CoG (fore and aft antenna) plot and are listed in Table 3.

**Table 3: ERS-2 Scatterometer anomalies in the CoG fore and aft antenna**

| Date | Reason |
|---|---|
| 26th and 27th September 1996 | missing on-board doppler coefficient (after cal. DC converter test period) |
| 6th and 7th June 1998 | no Yaw Steering Mode (after depointing anomaly) |
| 2nd and 3rd December 1998 | missing on-board doppler coefficients (after AMI anomaly 228) |
| 16th and 17th February 2000 | Fine Pointing Mode (FPM) (due to AOCS mono-gyro qualification period) |

The peaks shown in the plot of mid beam CoG standard deviation are linked to the satellite manoeuvres and AOCS anomaly.

The Figure 30 shows the daily mean of the CoG and CoG standard deviation before and during the qualification period. Figure 31 and Figure 32 show the averaged CoG per orbit before the qualification period while Figure 33 and Figure 34 show the averaged CoG per orbit during the qualification period. The large deviation in Figures 33 and 34 are relative to the orbits where the satellite was operated in FPM. As reported in the figures the CoG has a mean decrease (w.r.t the old AOCS) of roughly 200 Hz (300 Hz for the aft antenna) during the period 7th - 9th February and a mean increase (w.r.t. the old AOCS) of roughly 150 Hz (three antennae) from 10th February 2000 onwards. This difference is due to the selected gyro used to pilot the satellite. The gyro number 6 was selected in the first period while the gyro number 5 was selected in the second one. For the CoG standard deviation the high values on day 16th and 17th February are because the satellite was piloted with FPM.

The changes in the doppler frequency are due to pointing errors so the evolution of the CoG during one orbit gives qualitative information about the evolution of these error angles.

Figures 35, 36 and 37 shows the averaged CoG (mid antenna) as time function from the ascending node (time = 0). Each unit of the X axis is 5 seconds from the ascending node while the Y axis is the frequency in Hz. Figure 35 is relative to the qualification period with gyro 6, Figure 36 is relative to the qualification period with gyro 5 and Figure 37 is before the qualification period (AOCS with 3 gyroscopes). The solid line in the plots is the retrieved CoG from the values stored in the UWI products. These values have a frequency discretization of 234.4 Hz (as shown in the dotted line) that must be take into account to evaluate the CoG evolution. Due to the discetization is not possible to give an absolute level for the CoG. It is clear from the figures that the result for the mono-gyro configuration is more noisy than the 3-gyro configuration. There are also difference in the behaviour of gyro-6 and gyro-5.

The variation of the CoG are very well correlated with the evolution of the error angles as shown in Figure 38 (absolute orbit 25205). The maximum error coincides with the high variation of the CoG near the end of the orbit (around 5000-5500 s. from the ascending node). This pointing error is due to the sun blinding. In the South hemisphere, during the ascending passes, the Earth Sensor is blinding by the sun light and switched-off for few seconds causes the high pointing error. In the old AOCS configuration sun blinding data were discarded because the AOCS had 3-gyro as independently information. This explain because the high fluctuation of the CoG does not appear in Figure 37 (3-gyro).

The sun blinding is a seasonal effect. Its maximum is expected every year during the period 12$^{nd}$ January 26$^{th}$ February and with the new AOCS configuration it has a local impact in the sigma nought as reported in section 2.2.

In order to remove the noise from the CoG signal and to detect differences between the AOCS configurations, a low pass filter has been applied to the CoG evolution throughout the orbit. Figure 39 and Figure 40 show the result. Figure 39 compares the AOCS 3-gyro configuration CoG (solid line) with the AOCS gyro6 configuration (dotted line) while Figure 40 compares the AOCS gyro5 configuration. For reference the level of the CoG (3 gyro case) is shifted up to reach the zero doppler at the ascending node.

The mono-gyro configuration follows the sinusoidal pattern of the 3-gyro configuration with a good agreement in particular for the case with gyro6. The gyro 5 goes away from sinusoidal pattern around 1500 seconds after the ascending node (North pole) and this configuration seems more sensible to the sun blinding.

The new AOCS configuration although does not replicate the behaviour of the 3-gyro is however effective to maintain the nominal instrument calibration performance as reported in chapter 2.

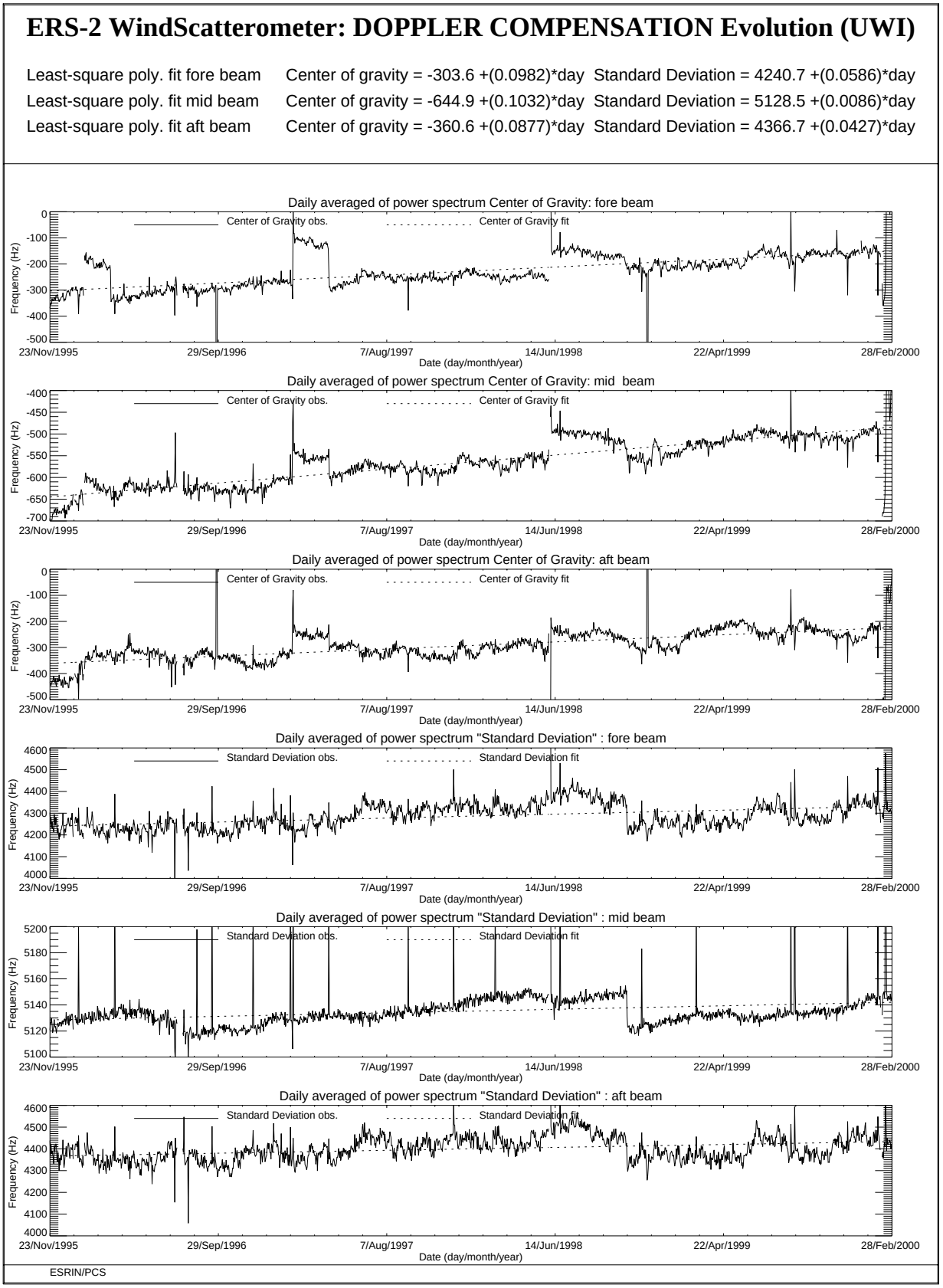


**FIGURE 29. ERS-2 Scatterometer: Centre of Gravity and standard deviation of received power spectrum since the beginning of the mission.**

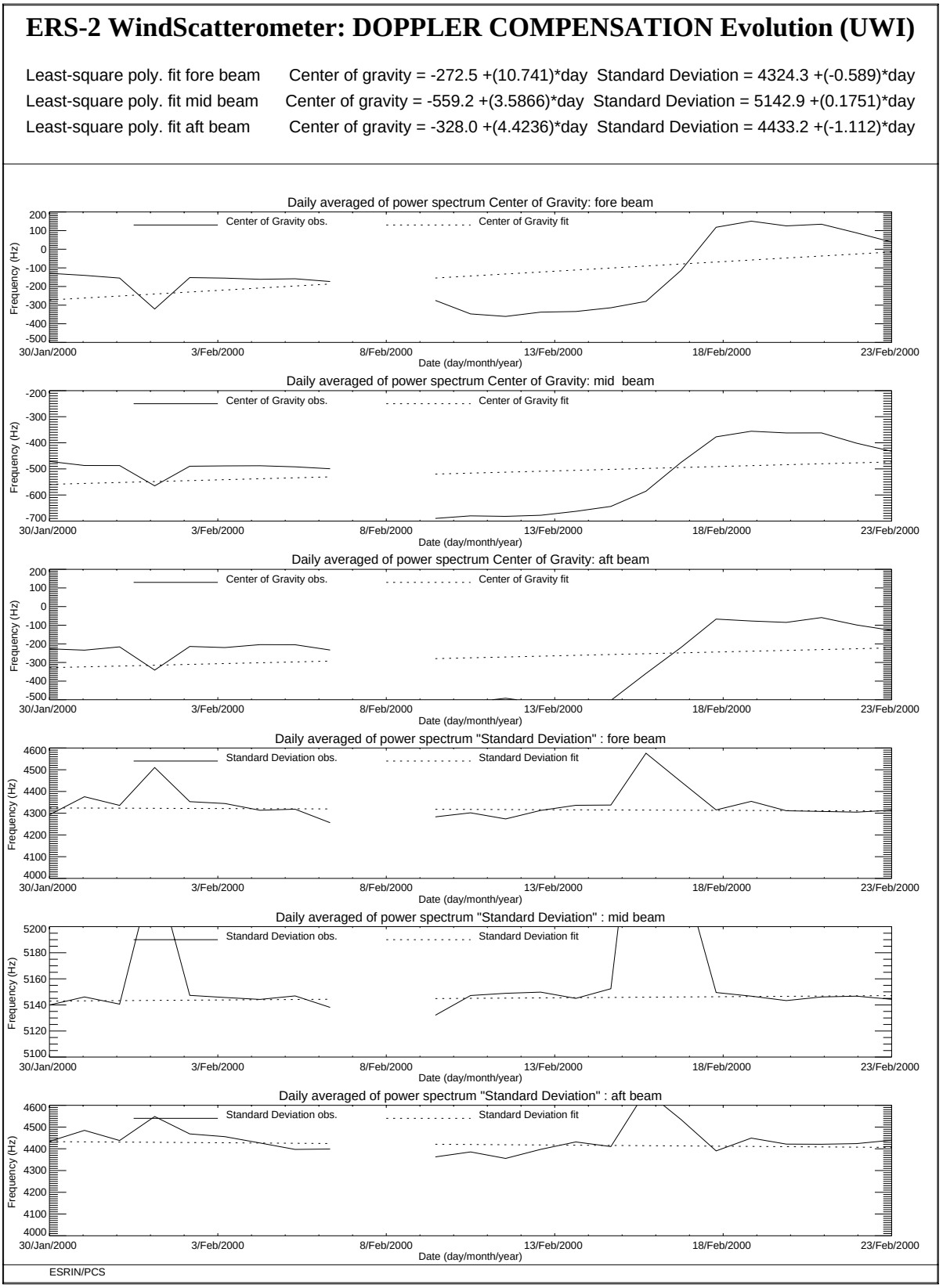


**FIGURE 30. ERS-2 Scatterometer: Centre of Gravity and standard deviation of received power spectrum during the AOCS mono-gyro qualification period.**

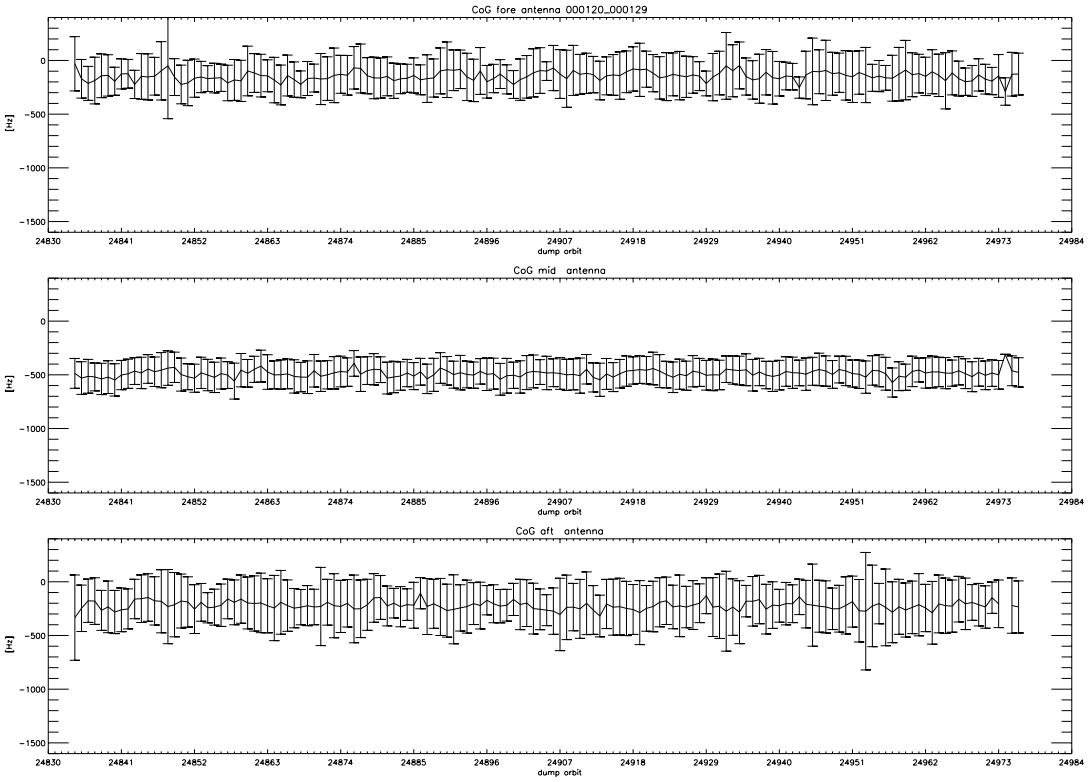


**FIGURE 31. CoG mean value and its error computed per orbit. Before the qualification period.**

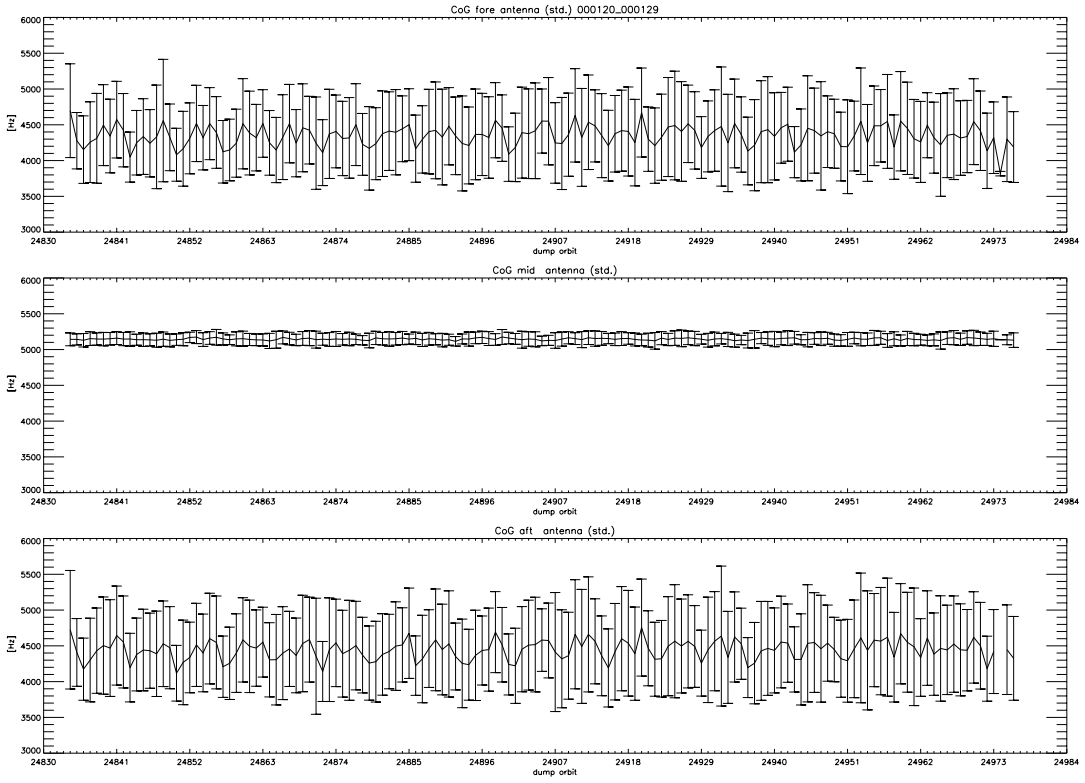


**FIGURE 32. CoG standard deviation value and its error computed per orbit. Before the qualification period.**

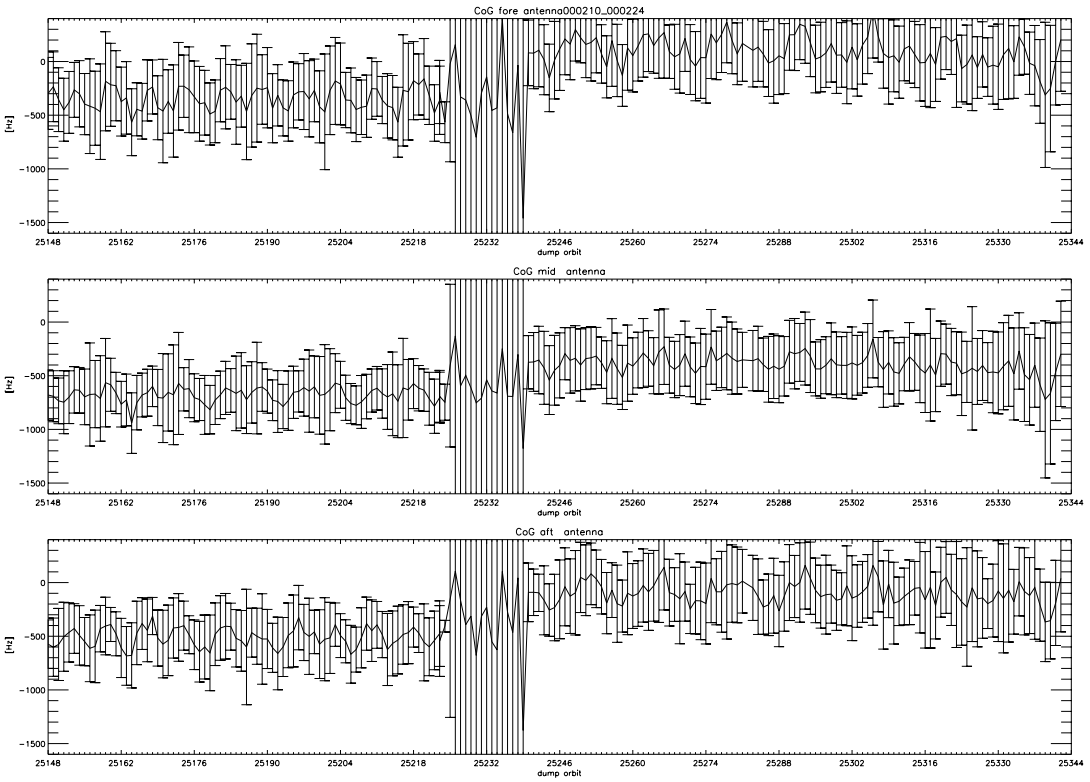


**FIGURE 33. CoG mean value and its error computed per orbit. Qualification period.**

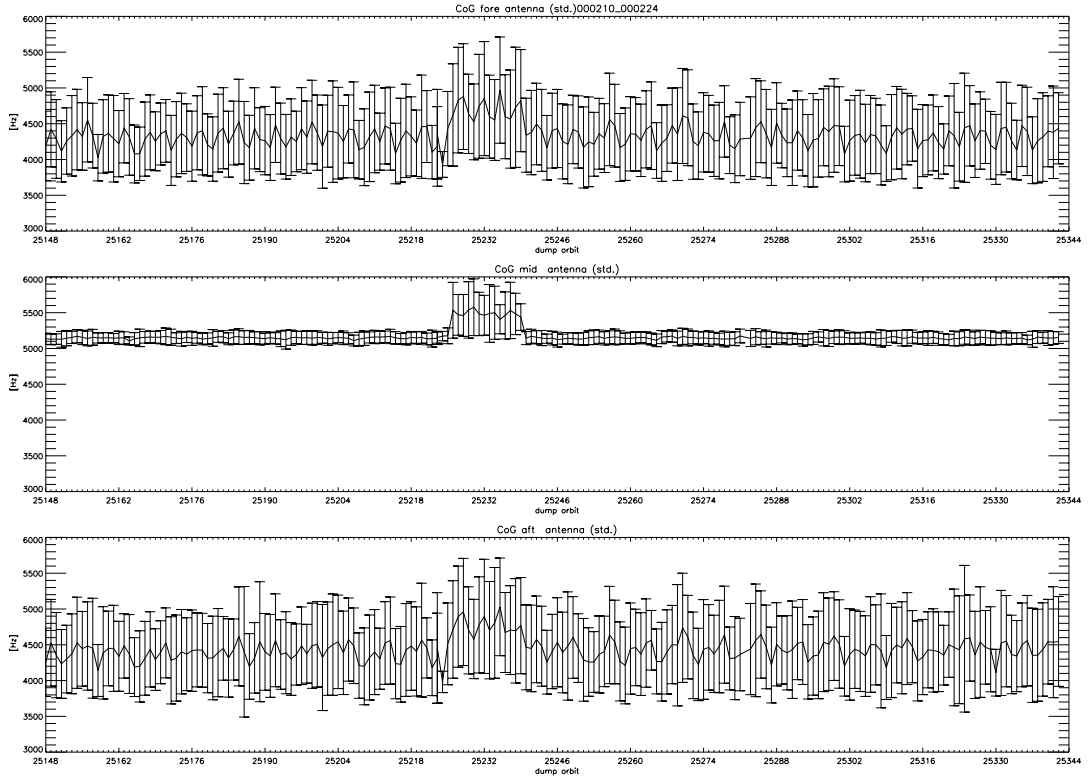


**FIGURE 34. CoG standard deviation and its error computed per orbit. Qualification period.**

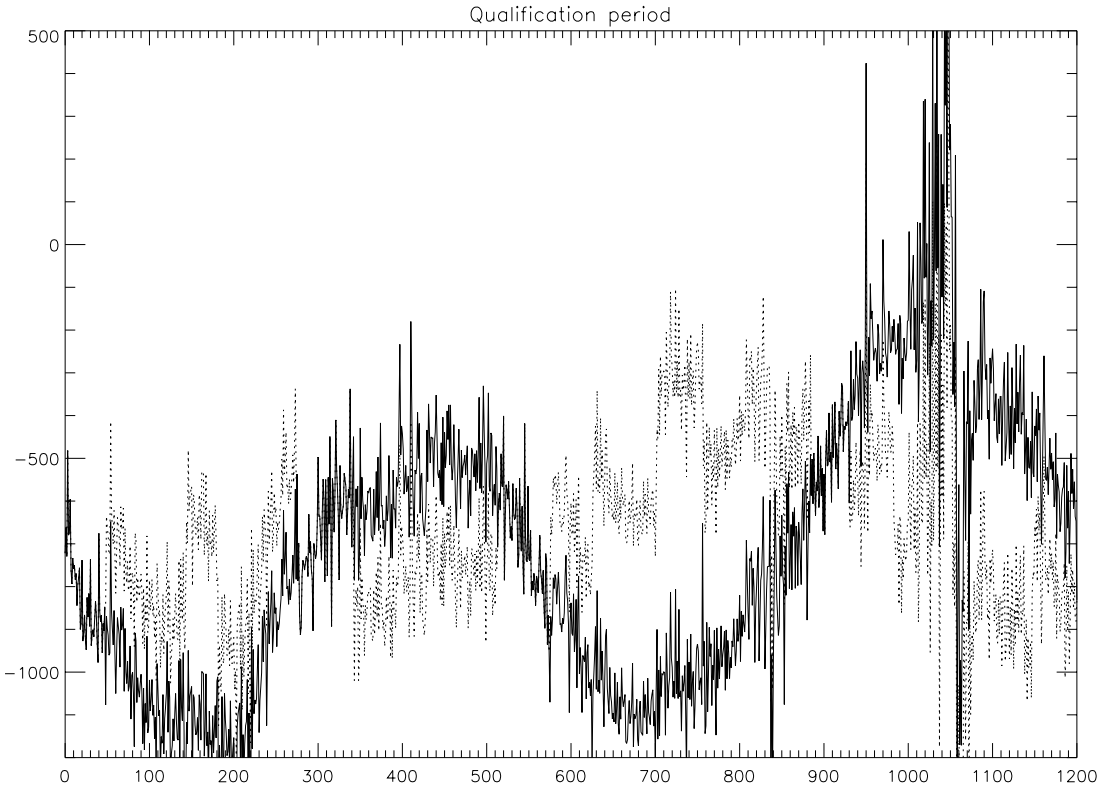


**FIGURE 35. Evolution of the Mid beam CoG from Ascending node time (1 unit = 5 s.) gyro=5.**

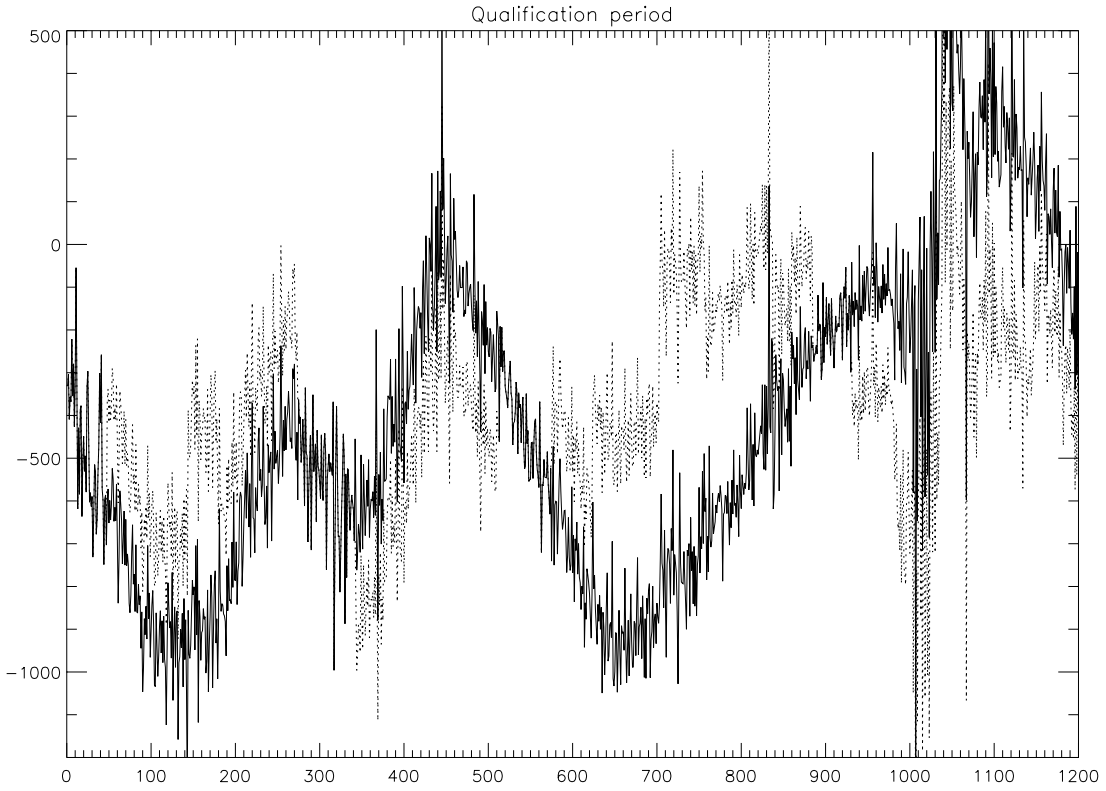


**FIGURE 36. Evolution of the Mid beam CoG from Ascending node time (1 unit = 5 s.) gyro=6**

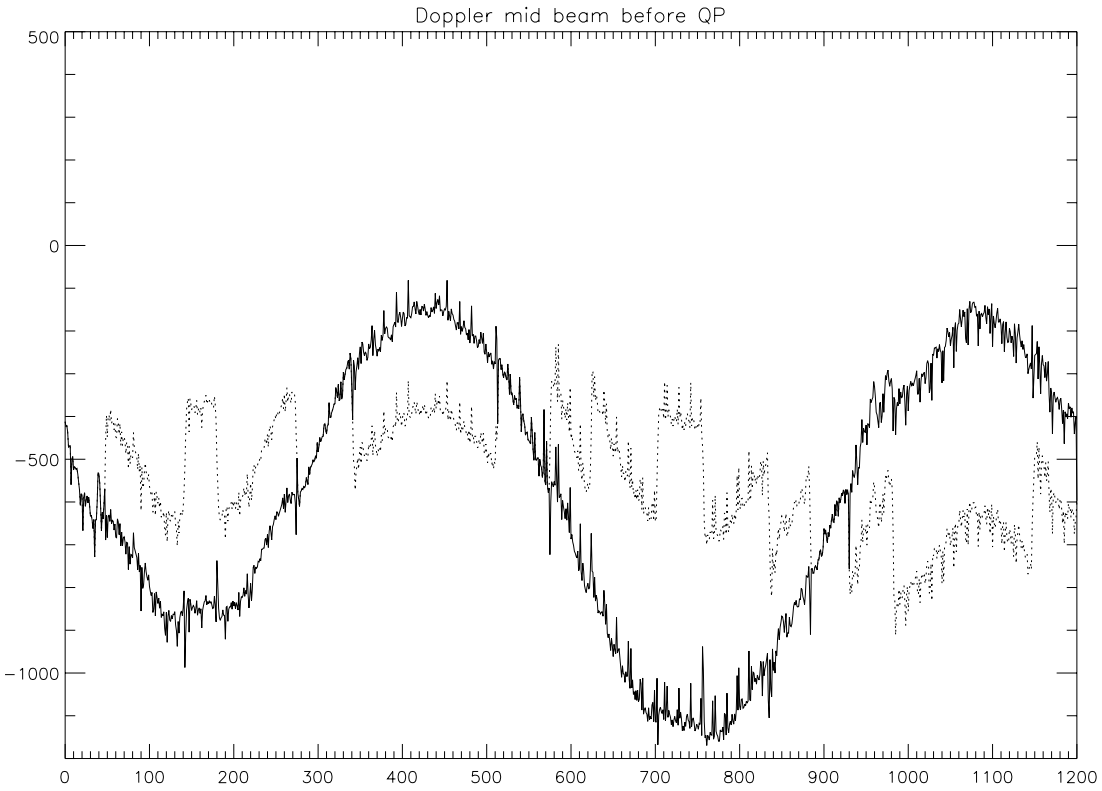


**FIGURE 37. Evolution of the Mid beam CoG from Ascending node time (1 unit = 5 s.). Before the qualification period, three gyro configuration.**

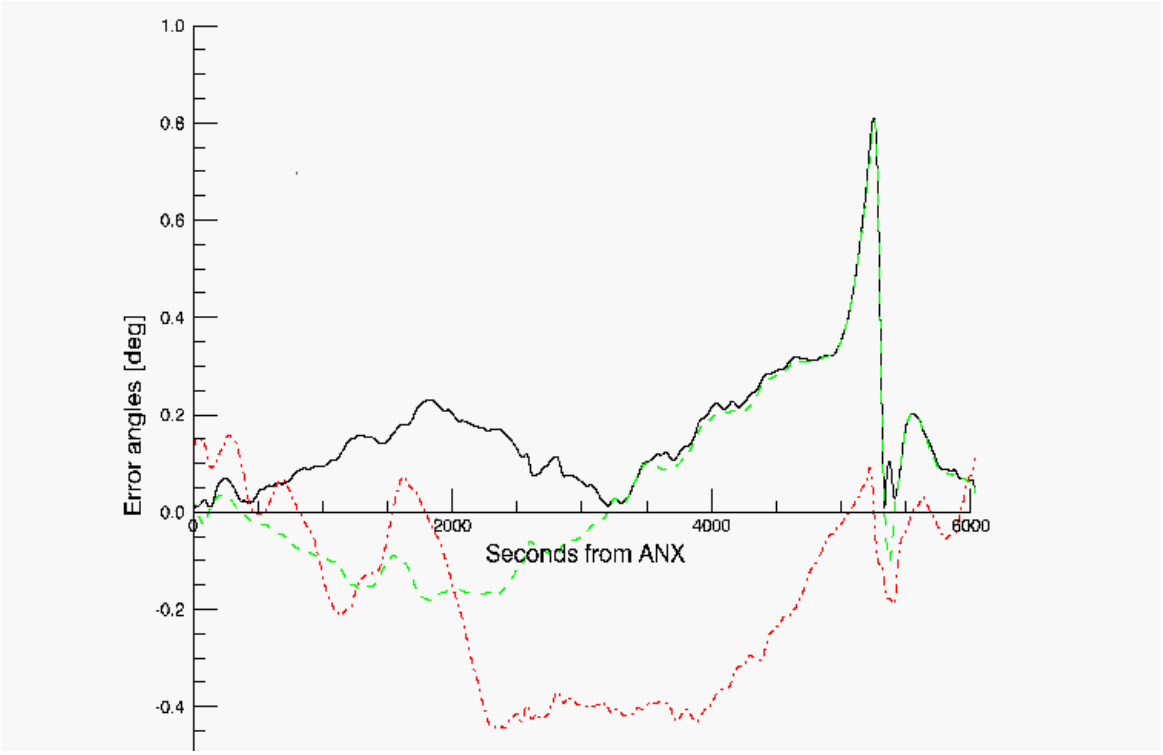


**FIGURE 38. Pointing error angles absolute orbit 25205**

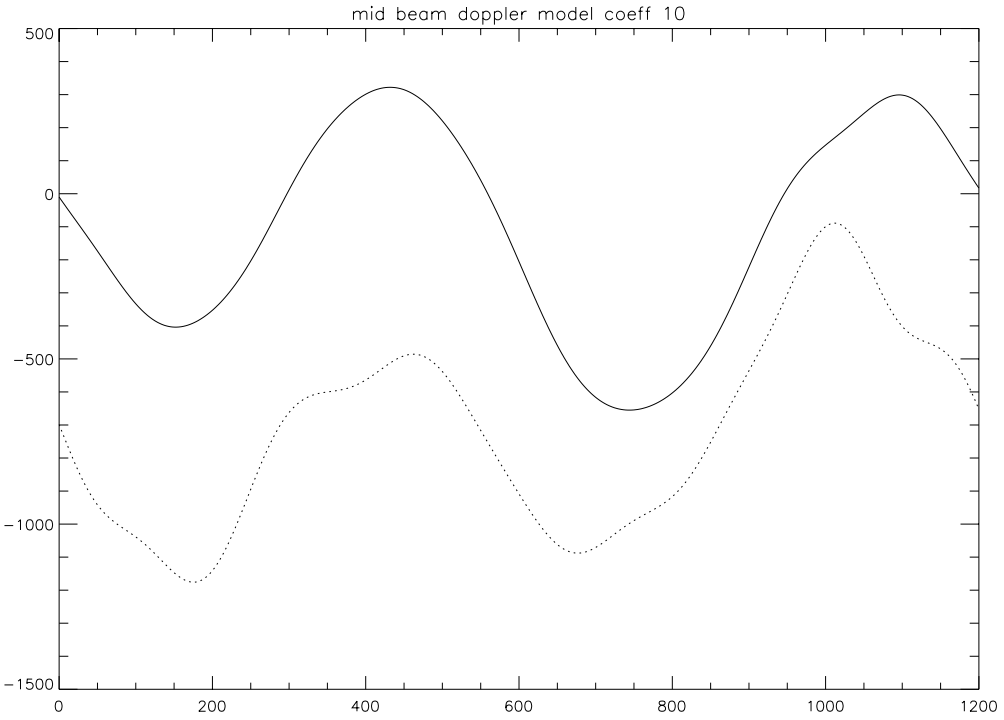


**FIGURE 39. Comparison between the three gyro configuration (solid line) and mono gyro (gyro=6) configuration. Low pass filtered evolution of the Mid beam CoG from Ascending node (1 unit = 5 s.).**

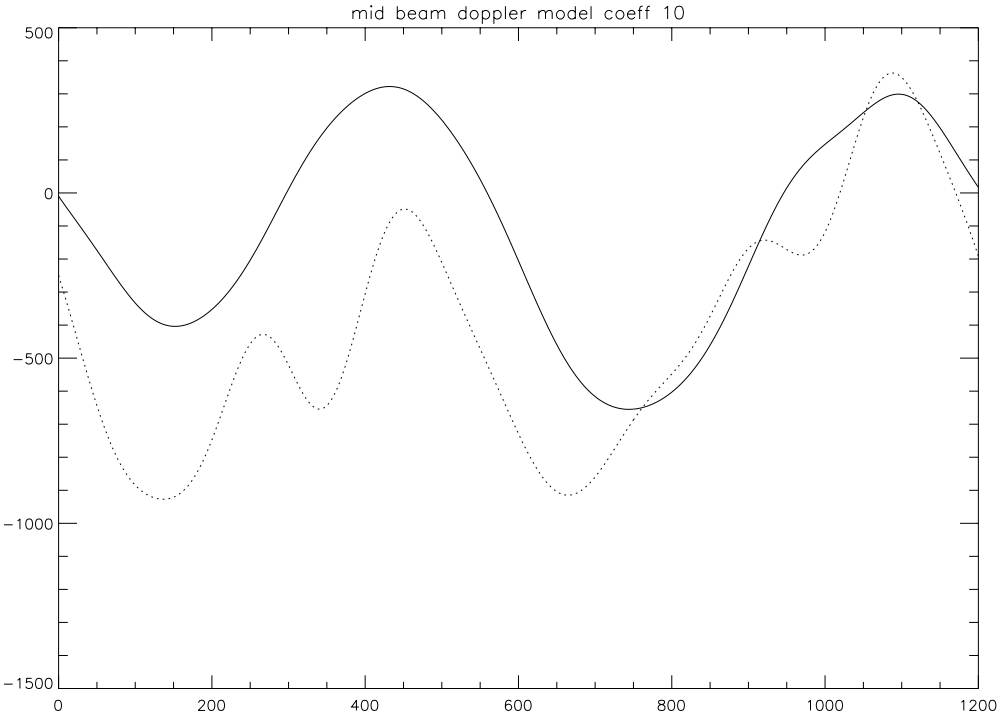


**FIGURE 40. Comparison between the three gyro configuration (solid line) and mono gyro (gyro=5) configuration. Low pass filtered evolution of the Mid beam CoG from Ascending node (1 unit = 5 sec)**

## 3.2 Noise power level I and Q channel

The results of the monitoring are shown in Figure 41. The first set of three plots presents the noise power evolution for the I channel while the second set shows the Q channel. The noise level is less than 1 ADC Unit for the fore and aft signals and is negligible for the mid one. From the plots one can see that the noise level is more stable in the I channel than in the Q one. The PCS suspects that an explanation should be found in the different position of the receivers, in particular it seems that the Q one is closer to the ATSR-GOME electronics. A confirmation of this hypothesis has been asked to ESTEC.

Since 5th December 1997 some high peaks appear in the plots. These high values for the daily mean are due to the presence for these special days of a single UWI product with an unrealistic value in the noise power field of the Specific Product Header. The analysis of the raw data used to generate these products lead in all cases to the presence of one source packet with a corrupted value in the noise field stored into the source packet Secondary Header. Table 4 presents the list of the UWI products affected by a corrupted noise field and disseminated during cycle 50.

**Table 4: UWI products with noise field corrupted (cycle 50)**

| Noise Field corrupted | Noise value (ADC Unit) | Acquisition Time |
|---|---|---|
| None | - | - |

The reason why noise field corruption is beginning from 5th December 1997 is at present unknown. It is interesting to note that at the beginning of December 1997, we started to get as well the corruption of the Satellite Binary Times (SBTs) stored in the EWIC product. The impact in the fast delivery products was the production of blank products starting from the corrupted EWIC until the end of the scheduled stop time. A change in the ground station processing in March 1998 overcame this problem.

Since 9th August 1998 some periods with a clear instability in the noise power have been recognised. Table 5 gives the detailed list.

**Table 5: ERS-2 Scatterometer instability in the noise power**

| From | To |
|---|---|
| 9th August 1998 | 26th October 1998 |
| 29th November 1998 | 6th December 1998 |
| 23rd December 1998 | 24th December 1998 |
| 7th June 1999 | 10th June 1999 |
| 17th August 1999 | 22nd August 1999 |
| 8th September 1999 | 9th September 1999 |
| 3rd October 1999 | 8th October 1999 |
| 16th October 1999 | 18th October 1999 |
| 26th October 1999 | 28th October 1999 |

| From | To |
|---|---|
| 25th December 1999 | 2nd January 2000 |
| 10th February 2000 | 11th February 2000 |

To better understand the instability of the noise power the PCS has carried out investigations in the scatterometer raw data (EWIC) to compute the noise power with more resolution. The result is that for the orbits affected by the instability the noise power had a decrease of roughly 0.7 dB for the fore and aft signals and a decrease of roughly 0.6 dB in the mid beam case (see report cycle 42). The decrease of the noise power during the orbits affected by the instability is comparable with the decrease of the internal calibration level that occurred during the same orbits. The reason of this instability (linked to the AMI anomalies) is still under investigation. A plot that shows the correlation among the noise power, the internal calibration level and the AMI anomaly is reported in section 3.3.

Figure 42 shows the evolution of the noise power since 26th October when 2 dB were added to the transmitted power. The periods with the instability in the noise are clear shown in the plots, in particular for the channel I plots (fore and aft beam).

During cycle50 the evolution of the noise power was stable apart from a couple of days after the AMI switch-on (10th February).

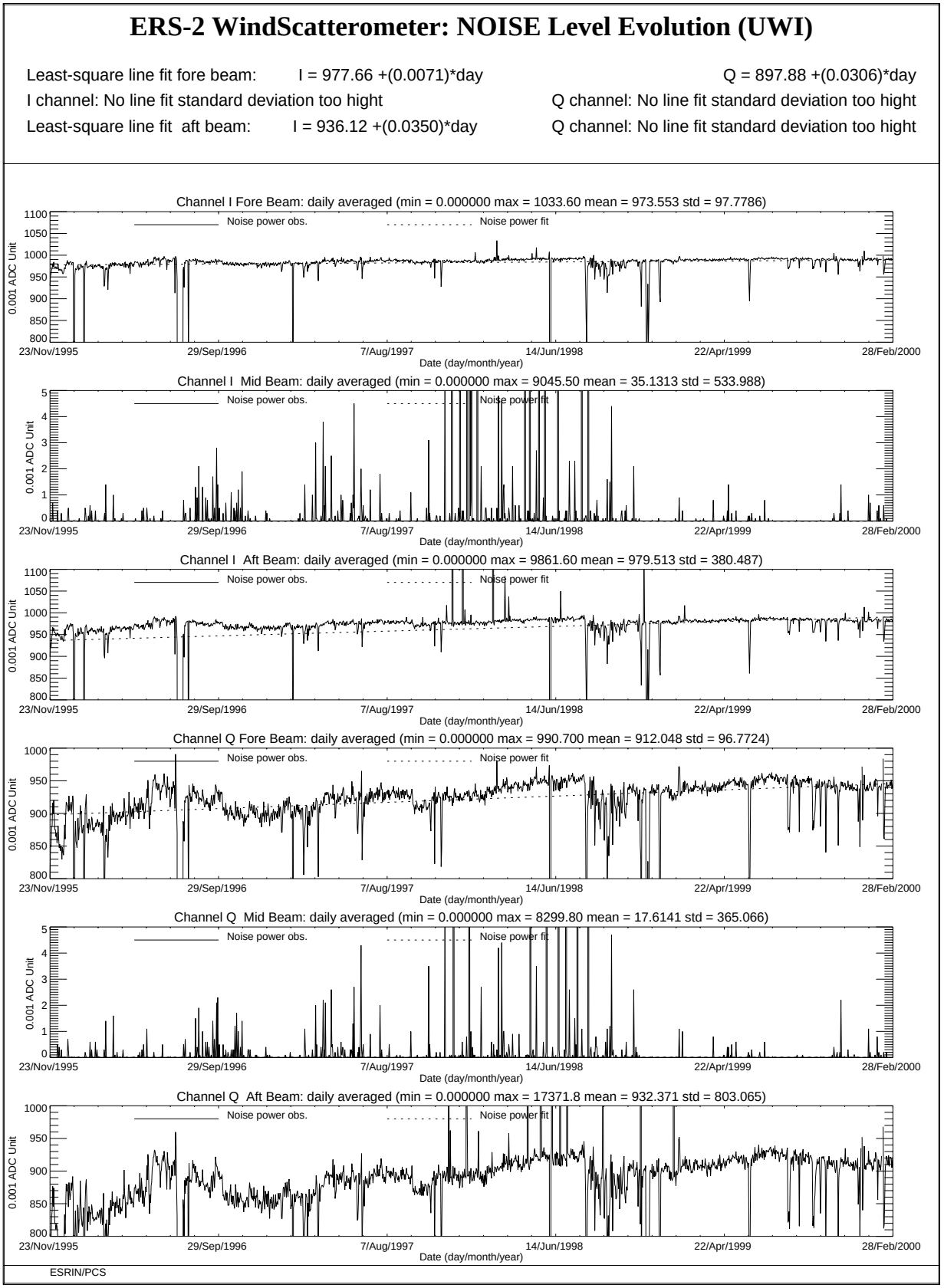


**FIGURE 41. ERS-2 Scatterometer: noise power I and Q channel since the beginning of the mission.**

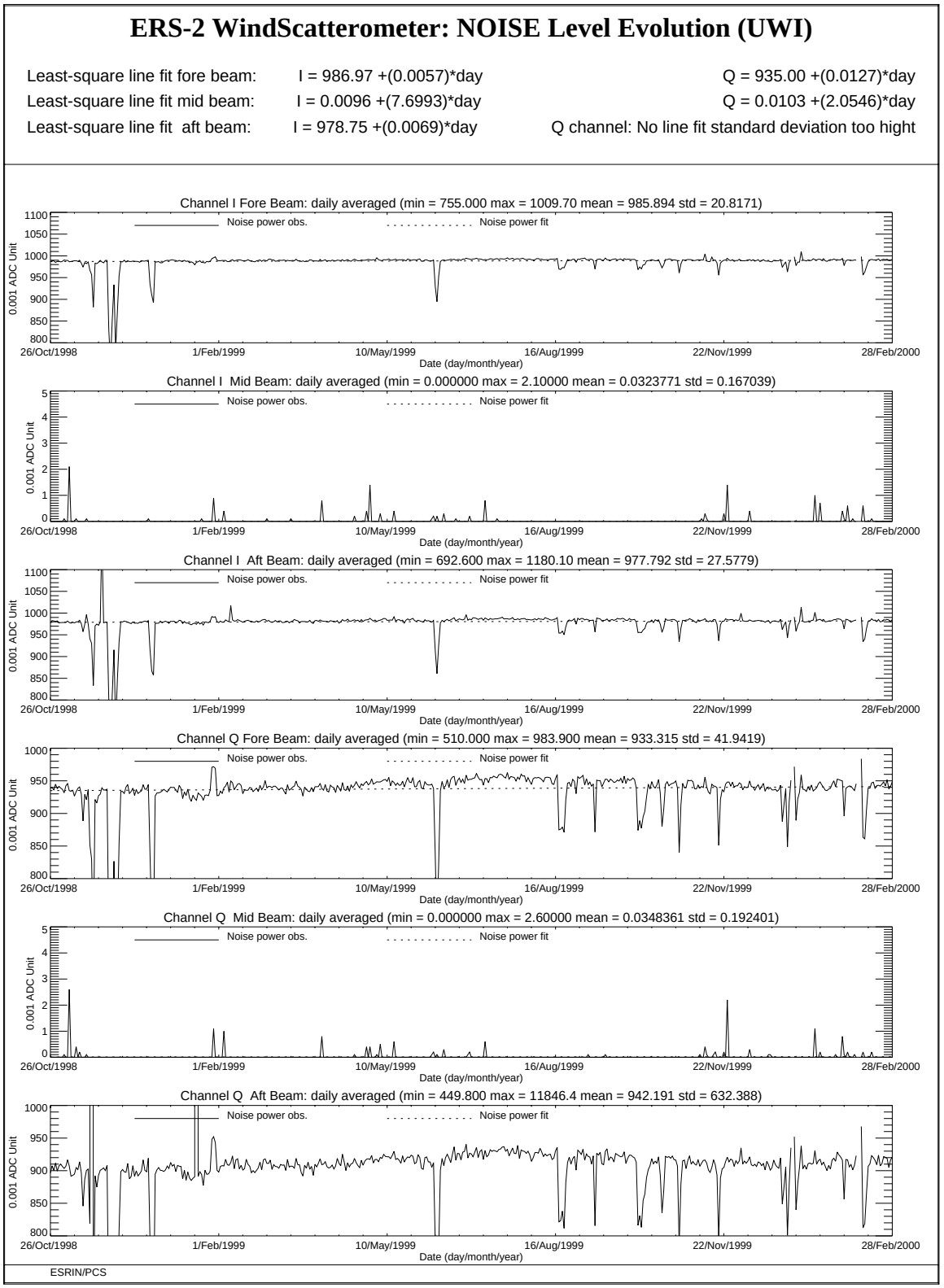


**FIGURE 42. ERS-2 Scatterometer: noise power I and Q channel since 26th October 1998 when the transmitted power was increased by 2 dB.**

## 3.3 Power level of internal calibration pulse

For the internal calibration level, the results, since the beginning of the mission, are shown in Figure 44.

The high value of the variance in the fore beam until August, 12th 1996 is due to the ground processing. In fact all the blank source packets ingested by the processor were recognized as fore beam source packets with a default value for the internal calibration level. The default value was applicable for ERS-1 and therefore was not appropriate for ERS-2 data processing. On August 12th, 1996 a change in the ground processing LUT overcame the problem.

Since the beginning of the mission a power decrease is detected. The reason is that the TWT is not working in saturation, so that a variation in input signal is visible in output. The variability of the input signal can be two-fold: the evolution of the pulse generator or the tendency of the switches between the pulse generator and the TWT to reset themselves into a nominal position. These switches were set into an intermediate position in order to put into operation the scatterometer instrument (on 16th November 1995). The decrease is estimated to be about 0.0025 dB per day. After the change of the calibration subsystem on August 6th, 1996 the decrease is more evident and it is estimated in 0.09 dB per cycle. The power decrease is regular and affects the AMI when it is working in wind-only mode, wind/wave mode and image mode indifferently.

On 26th October 1998 (cycle 37) to compensate for this decrease, 2.0 dB were added to the Scatterometer transmitted power and this explains the large step shows in Figure 43 and Figure 44. After that day the power decrease is on average 0.07 dB per cycle.

It is important to point out the efficiency of the internal calibration for keeping the absolute calibration level stable. In fact, no important change is noted in the monitoring of the gamma-nought level over the Brazilian rain forest during the power decrease and after the increase of the transmitted power (see section 2.0).

The internal calibration level shows an instability since 9th August 1998 that is very well correlated with the instability in the noise power as outlined in section 3.2.

Figure 43 shows the daily average of the internal calibration and the noise power from 1st August 1998 to 24th January 2000. In the figure are also reported the anomalies that affected the AMI (the triangles in the plot) and the days when the instability was very strong (asterisks in the plot). From Figure 43 it seems that there is a clear correlation between the instability and the AMI anomalies.

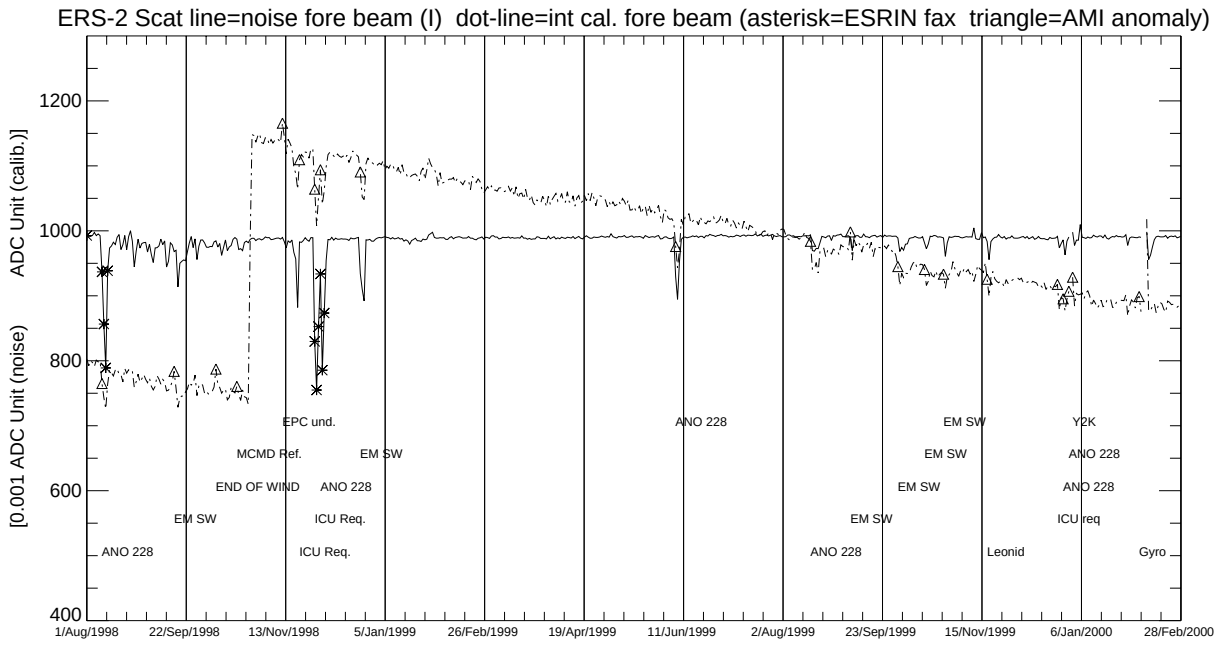


**FIGURE 43. ERS-2 Scatterometer: noise power (I channel fore antenna) and internal calibration power (fore antenna) evolution from 1st August 1998 to 28th February 2000.**

During the cycle 50 the internal calibration level had, on average, a power decrease of 0.028 dB.

Apart from the AMI anomalies the power decrease since 26th October 1998 is regular and it is on average 0.07 dB per cycle as shown in Figure 44.

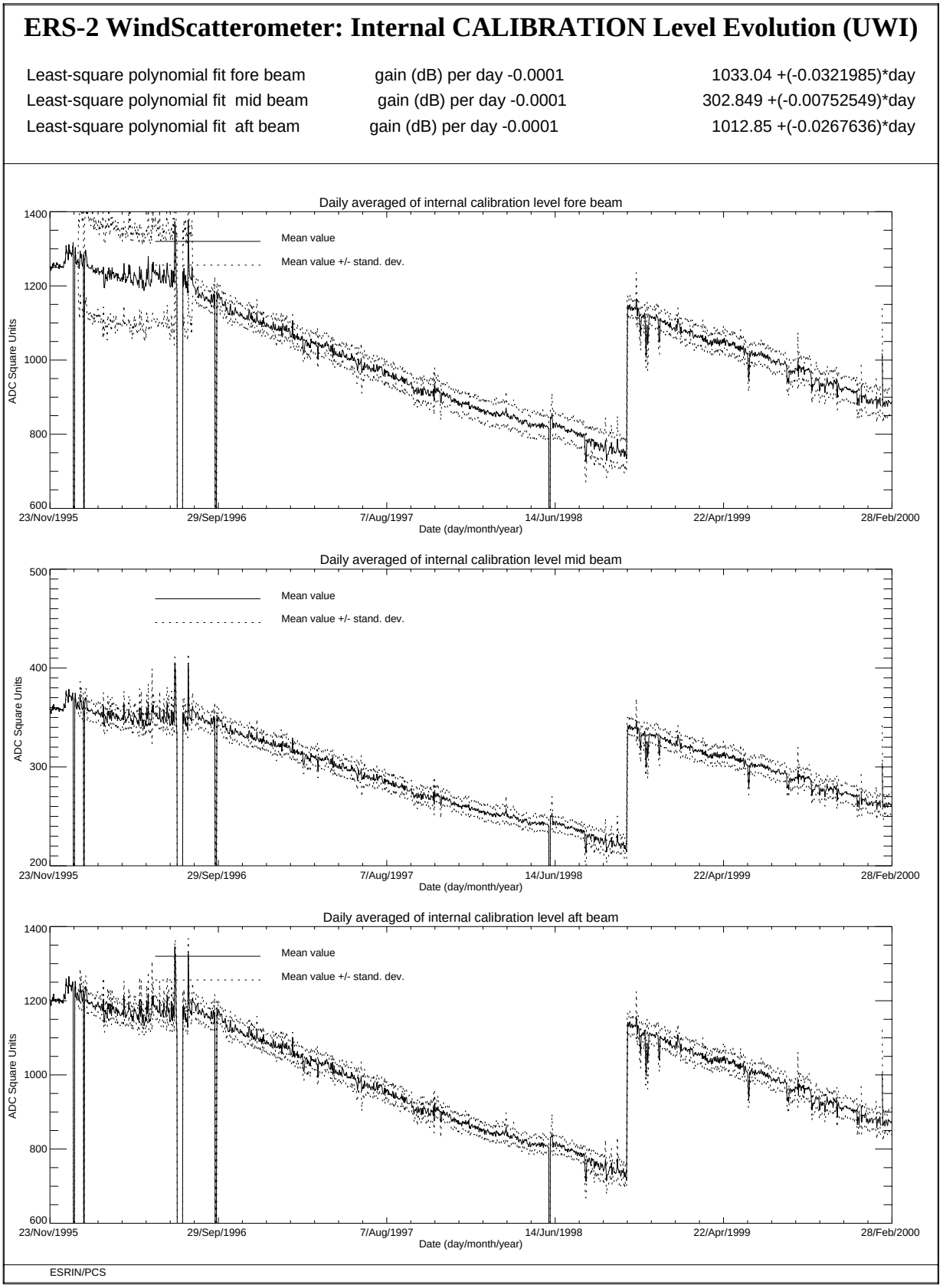


**FIGURE 44. ERS-2 Scatterometer: power of internal calibration pulse since the beginning of the mission.**

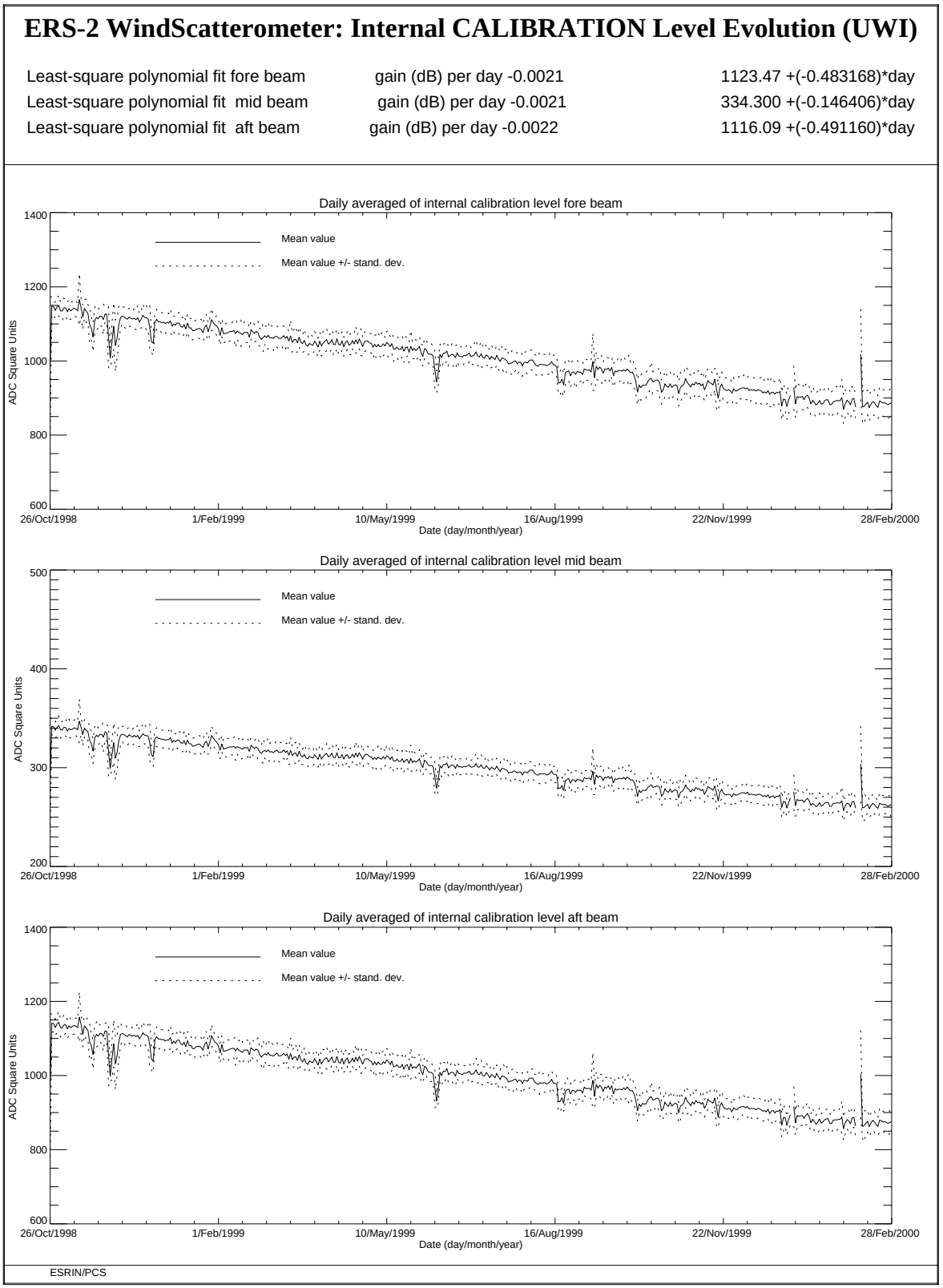


**FIGURE 45. ERS-2 Scatterometer: power of internal calibration level since 26th October 1998 when the transmitted power was increased by 2.0 dB.**

# 4.0 Products performance

One of the most important point in the monitoring of the products performance is their availability. The Scatterometer is a part of ERS payload and it is combined with a Synthetic Aperture Radar (SAR) into a single Active Microwave Instrument (AMI). The SAR users requirements and the constraints imposed by the on-board hardware (e.g. amount of data that can be recorded in the on-board tape) set rules in the mission operation plan.

The principal rules that affected the Scatterometer instruments are:

- over the Ocean the AMI is in wind/wave mode (scatterometer with small SAR imagettes acquired every 30 sec.) and the ATSR-2 is in low rate data mode.
- over the Land the AMI is in wind only mode (only scatterometer) and the ATSR-2 is in high rate mode. (Due to on board recorder capacity, ATSR-2 in high rate is not compatible with Sar wave imagette acquisitions.)

This strategy preserves the Ocean mission.

Moreover:

- the SAR images are planned as consequence of users' request.

These rules have an impact on the Scatterometer data availability as shown in Figure 46.

Each segment of the orbit has different colour depending on the instrument mode: brown for wind only mode, blue for wind-wave mode and green for image mode. The red and yellow colours correspond to gap modes (no data acquired). The major problems came from the orbit segments between Australia and Antarctic and between Africa and Antarctic where a lot of data are not acquired. This problem is under investigation by ESRIN and a new mission operation plan for the scatterometer shall be adopted.

For cycle 50 the percentage of the ERS-2 AMI activity is shown in table 6.

**Table 6: ERS-2 AMI activity (cycle 50)**

| AMI modes | ascending passes | descending passes |
|---|---|---|
| Wind and Wind-Wave | **85.8%** | **80.2%** |
| Image | **1.8%** | **5.8%** |
| Gap and others | **12.4%** | **14.0%** |

The percentage of scatterometer activity during the cycle 50 was less than the nominal value because the ERS-2 payloads were switched-off to uplink the new AOCS configuration software. This explains the orbit missing in Figure 46.

Table 7 reports the major data lost due to the test periods and AMI or satellite anomalies occurred after August 6th, 1996 (before of this day for many times data were not acquired due to the DC converter failure).

**Table 7: ERS-2 Scatterometer mission major data lost after 6th, August 1996**

| From | To | Reason |
|---|---|---|
| September 23rd, 1996 | September 26th, 1996 | ERS-2 switched off due to a test period |
| February 14th, 1997 | February 15th, 1997 | ERS-2 switched off due to a depointing anomaly |
| June 3rd, 1998 | June 6th, 1998 | ERS-2 switched off due to a depointing anomaly |
| November 17th, 1998 | November 18th, 1998 | ERS-2 switched off to face out Leonide meteo storm |
| September 22nd 1999 | September 23rd 1999 | ERS-2 switched off due to Year 2000 certification test |
| November 17th, 1999 | November 18th, 1999 | ERS-2 switched off to face out Leonide meteo storm |
| December 31st,1999 | January 2nd, 2000 | ERS-2 switched off Y2K transition operation |
| February 7th,2000 | February 9th, 2000 | ERS-2 switched off due to new AOCS s/w up-link |

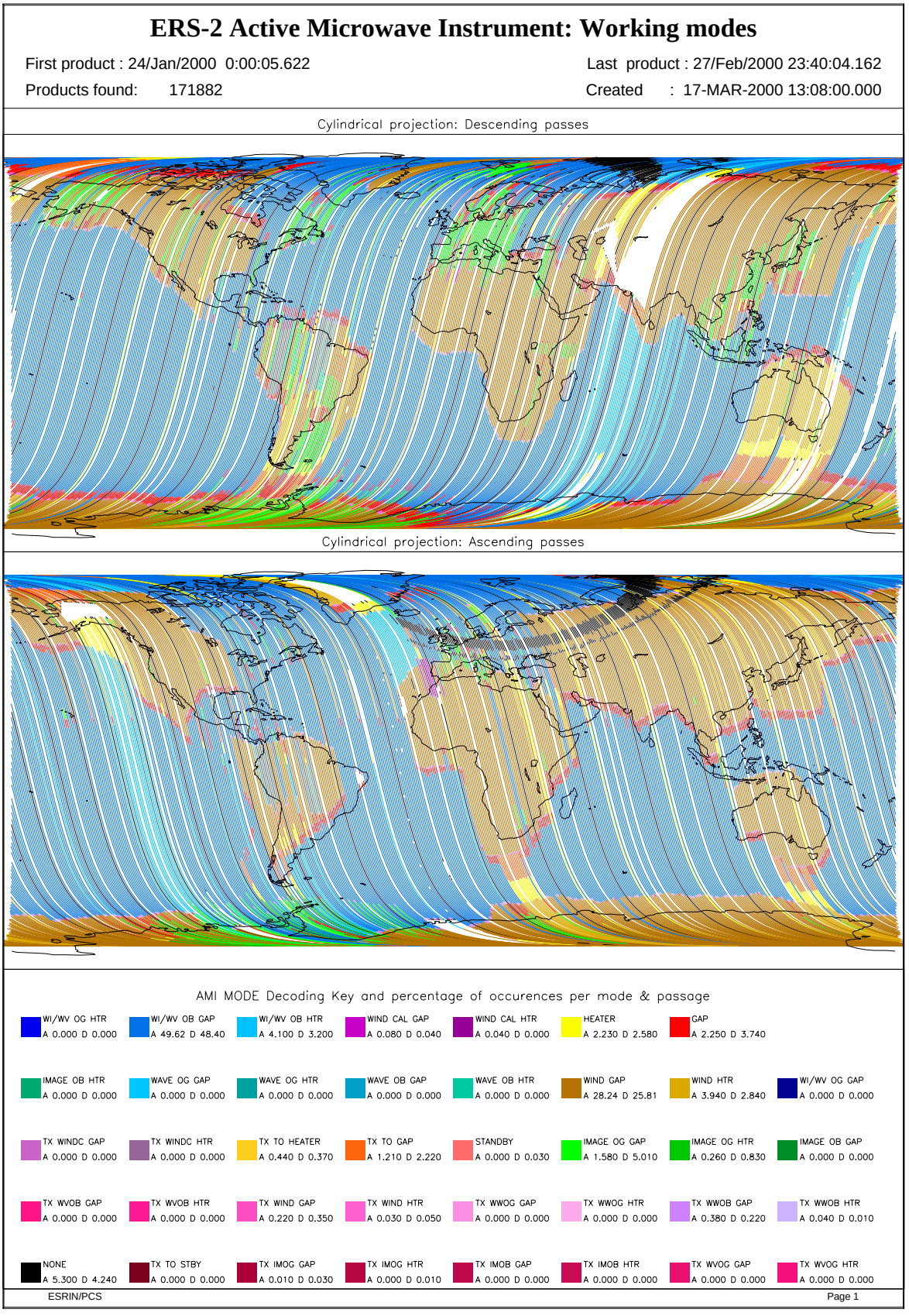


**FIGURE 46. ERS-2 AMI activity during cycle 50.**

The PCS carries out a quality control of the winds generated from the WSCATT data. The activity is split in two main areas: the first one includes a routine analysis of the fast Delivery Products disseminated to the users, the second one is focused on the improvement of the CMOD-4 (the operative ESA wind retrieval algorithm) for high wind speed (for more information see on the Web site http//pcswww.esrin.esa.it the Cyclone Tracking home page). External contributions to this quality control come also from ECMWF and UK-Met Office.

The routine analysis is summarized in the plots of figure 25; from top to bottom:

- the monitoring of the valid sigma-nought triplets per day.
- the evolution of the wind direction quality. The ERS wind direction (for all nodes and only for those nodes where the ambiguity removal has worked properly) is compared with the ECMWF forecast. The plot shows the percentage of nodes for which the difference falls in the range -90.0, +90.0 degrees.
- the monitoring of the percentage of nodes whose ambiguity removal works successfully.
- the comparison of the wind speed deviation: (bias and standard deviation) with the ECMWF forecast.

The results since the beginning of the mission can be summarized (after August 6$^{th}$, 1996 and apart from the events given in Table 7) as:

- a stable number of valid sigma-nought with a small increase after June 29$^{th}$, 1999 due to the dissemination in fast delivery of the data acquired in the Prince Albert station.
- an accurate wind direction for roughly 93% of the nodes, a success in the ambiguity removal for more than 90.0% of the nodes.

The ERS-2 wind speed shows an absolute bias of roughly 0.5 m/s and a standard deviation that ranges from 2.5 m/s to 3.5 m/s with respect to the ECMWF forecast. The wind speed bias and its standard deviation have a seasonal pattern due to the different winds distribution between the winter and summer season.

It is important to note that only after the end of calibration phase (mid March 1996) the wind products have reached high quality.

Two important changes affect the speed bias plot: the first is on June 3$^{rd}$, 1996 and it is due to the switch from ERS-1 to ERS-2 data assimilation in the meteorological model. The second change, which occurred at the beginning of September 1997, is due to the new monitoring and assimilation scheme in ECMWF algorithms (4D-Var).

Since 19$^{th}$ April 1999 two set of meteo-table (meteorological forecast centred at 00:00 and 12:00 of each day) are used in the ground processing. With this new strategy the data are processed using the 18 and 24 hours meteorological forecast instead of the 18, 24, 30 36 hours forecast. The data processed with the 18-24 hours tables instead of 30-36 hours tables have an increase in the number of ambiguity removed nodes but no important improvements are shown, on average, in the daily statistics.

Since 25$^{th}$ August 1999 a new LRDPF software (version 8500) is operative in the ground stations. With this upgrade the LRDPF is year 2000 compatible; no changes were introduced in the scatterometer data processing.

For cycle 50 the PCS quality control has reported stable results apart from 7th February to 10th February 2000 when the ERS-2 payloads were switched off to up-link the new AOCS software and no wind data were available. The quality of the wind was bad on days 16th and 17th February because the satellite was piloting in FPM that is less accurate of the nominal mode.

The Figure 47 shows the distance of the sigma nought triplets from the cone (Geophysical model) before and during the qualification period. As reported in the figure the sigma nought triplets acquired during the qualification period have a distance from the cone very similar to the ones acquired with the 3-gyro AOCS configuration.

Figure 48 shows the wind data quality during the qualification period. As reported in the plots the new AOCS configuration did not affect the wind quality. The wind speed bias (UWI -ECMWF Forecast) is close to 0 m/s and the wind speed standard deviation is roughly 2.5 m/s. The ambiguity removal rate is above the 90%.

Figure 49 and 50 show the comparison between UWI products and meteorological analysis (First Guess) before and during the qualification period. The wind speed bias is ranging from -1.0 to 0.0 m/s while the wind direction bias is close to 0.0 degrees and, on global scale, there are not difference between the 3-gyro and mono-gyro AOCS configuration. To investigate the effect of the sun blinding wind statistics has been requested to ECMWF in the area 45-55 degrees South.

Figure 51 summarise the wind data performance since the beginning of the mission.

.

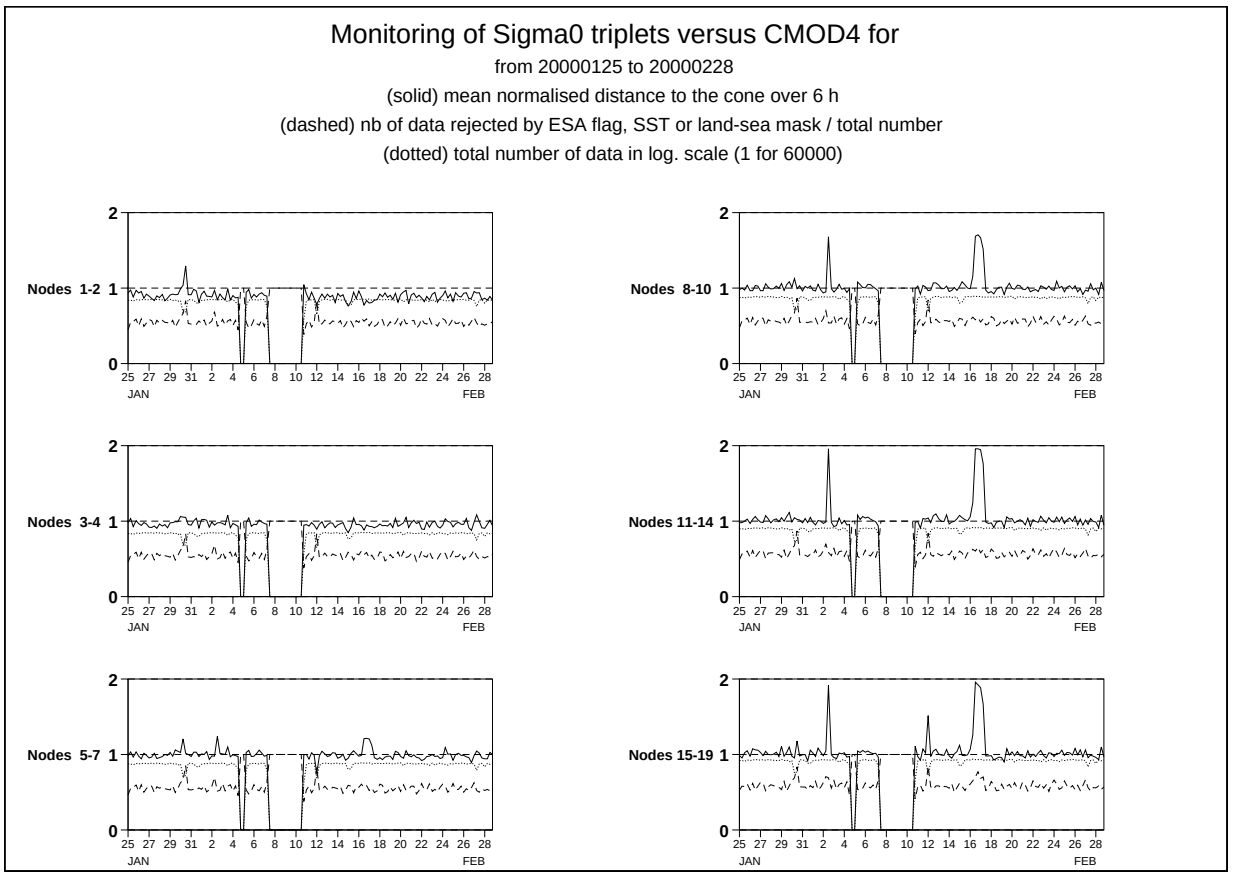


**FIGURE 47. ERS-2 WIndscatterometer sigma nought triplets: distance from the cone.**

.

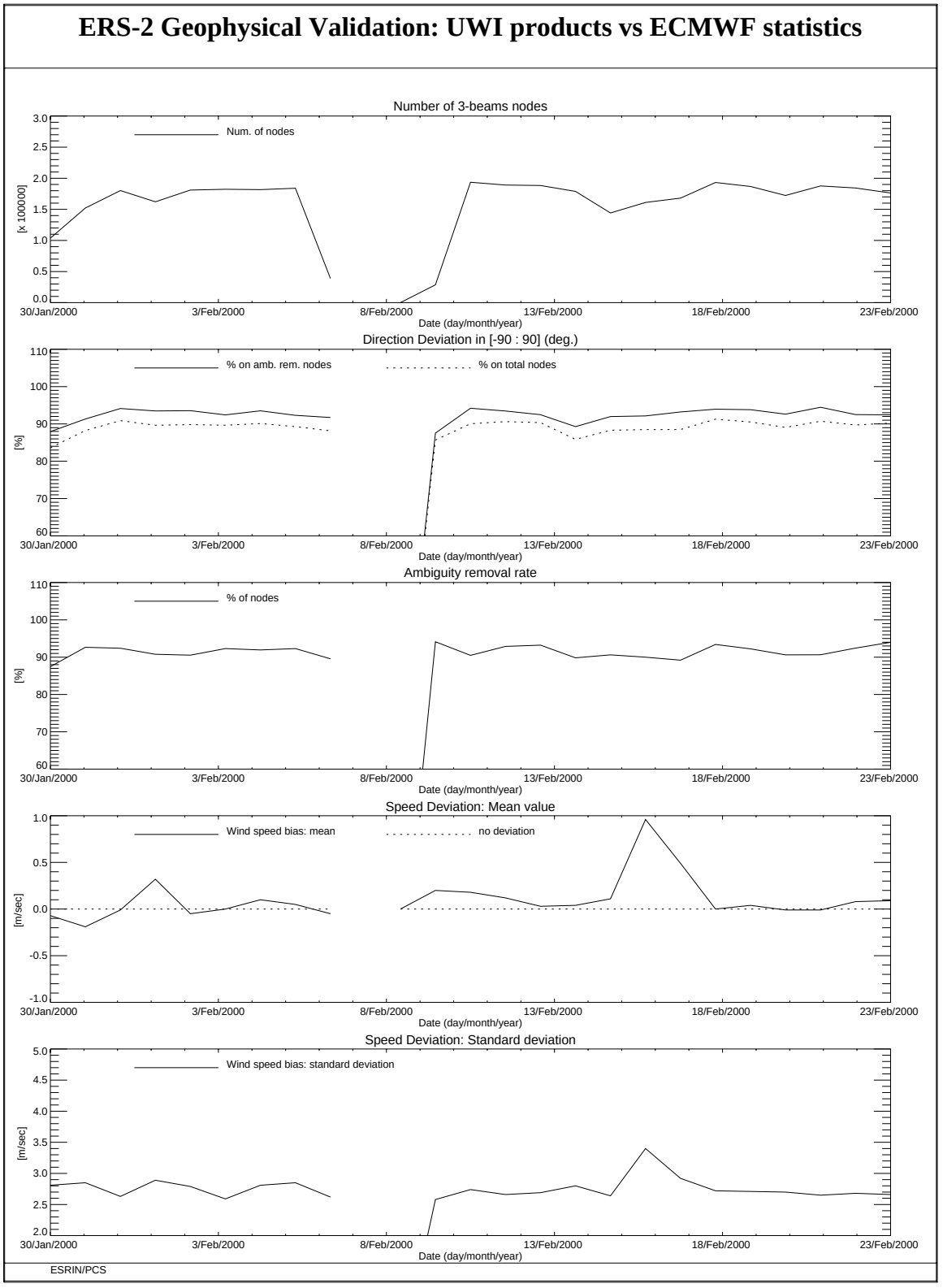


**FIGURE 48. ERS-2 WindScatterometer: Geophysical validation during the mono-gyro qualification period**

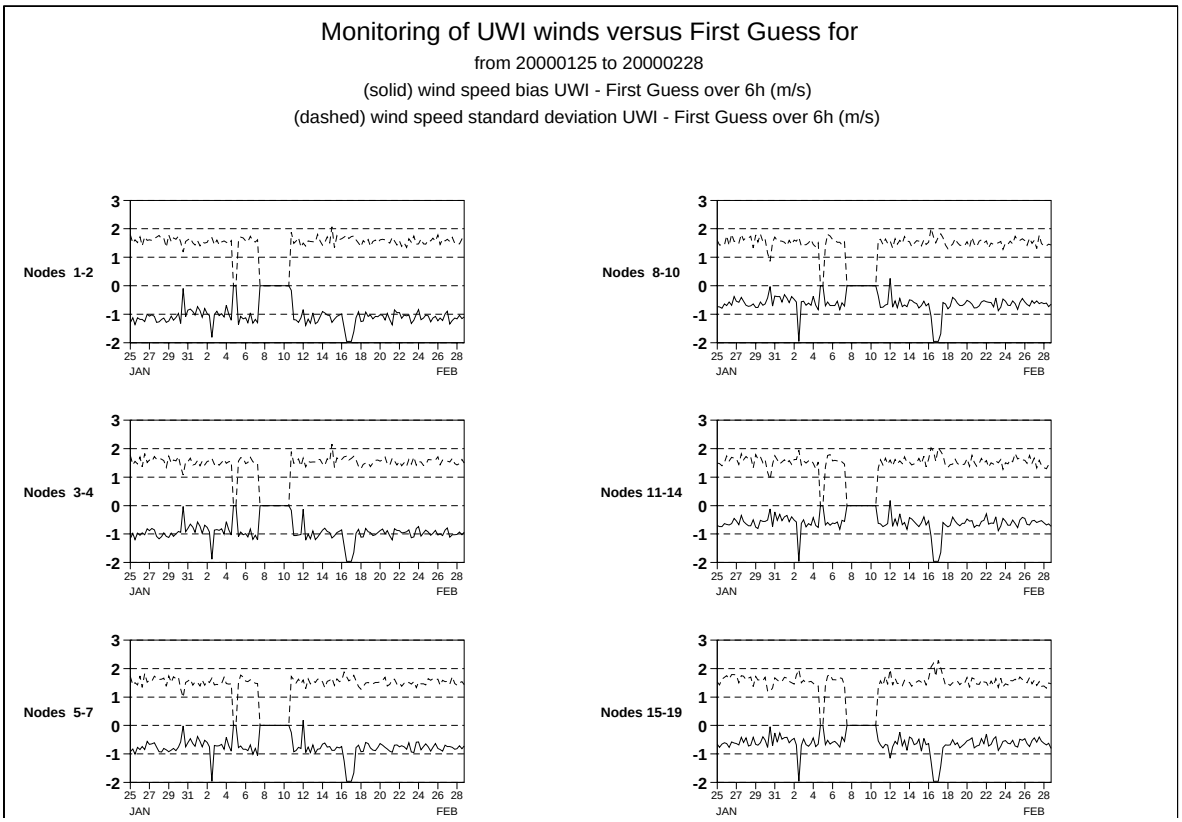


**FIGURE 49. ECMWF geophysical validation wind speed bias cycle 50**

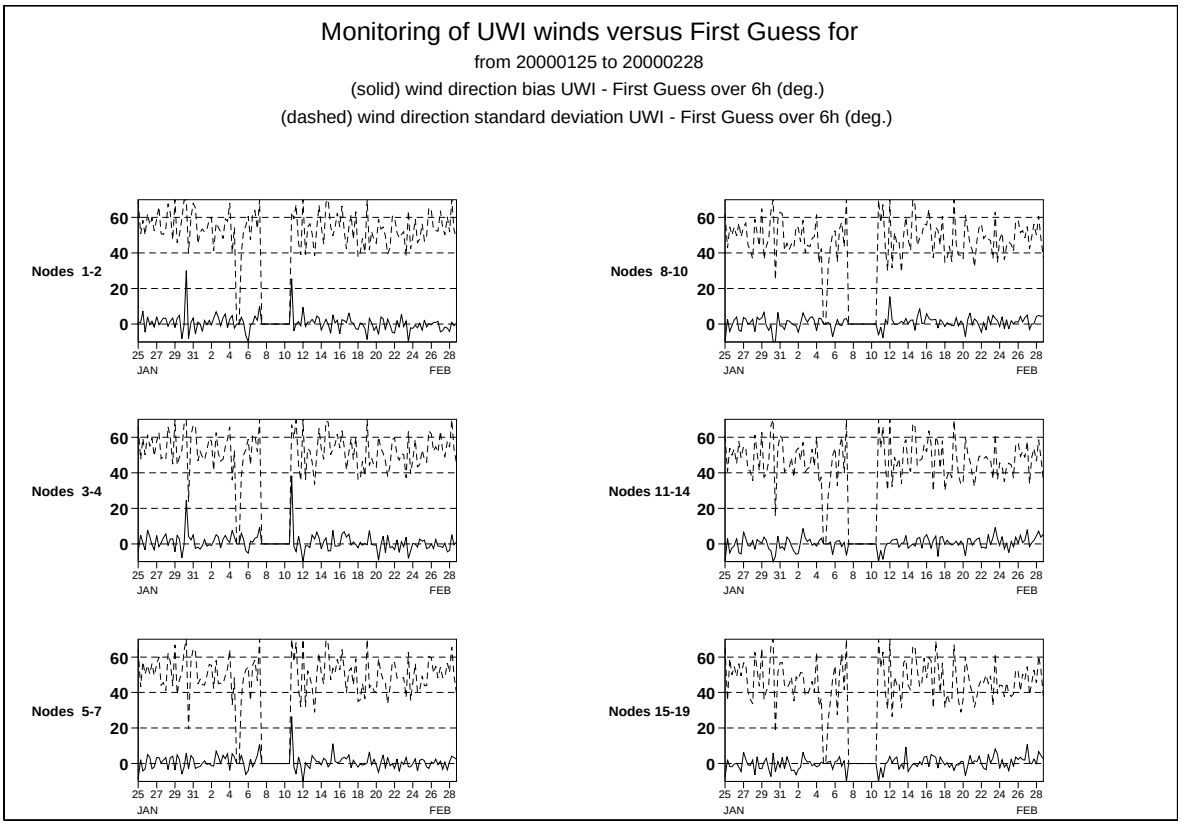


**FIGURE 50. ECMWF geophysical validation wind direction bias cycle 50**

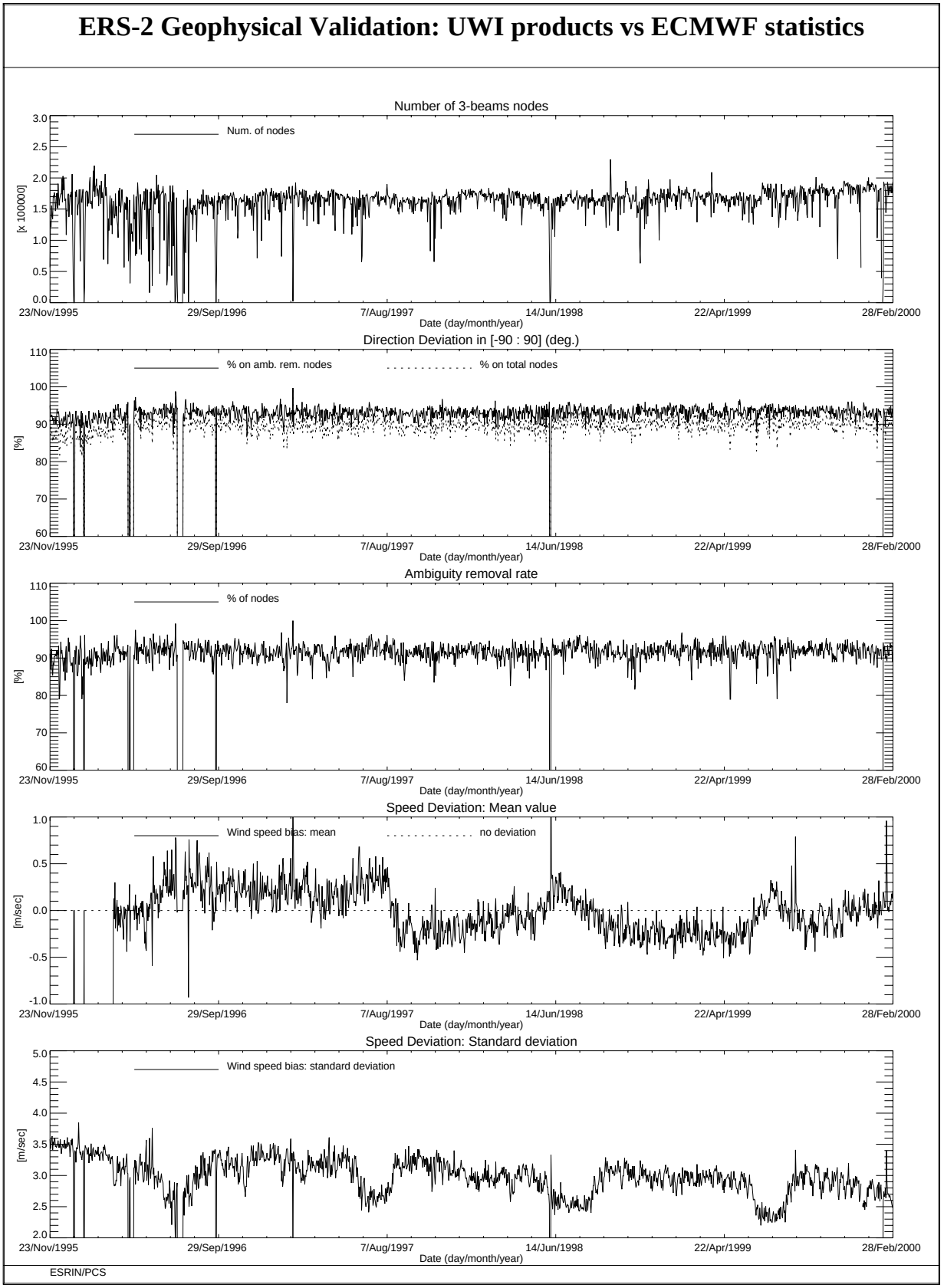


**FIGURE 51. ERS-2 Scatterometer: wind products performance since the beginning of the mission.**